

# An Evaluation of the Two-Dimensional Gabor Filter Model of Simple Receptive Fields in Cat Striate Cortex

JUDSON P. JONES AND LARRY A. PALMER

*Department of Anatomy, and David Mahoney Institute of Neurological Sciences,  
University of Pennsylvania School of Medicine, Philadelphia, Pennsylvania 19104-6058*

## SUMMARY AND CONCLUSIONS

1. Using the two-dimensional (2D) spatial and spectral response profiles described in the previous two reports, we test Daugman's (7) generalization of Marcelja's hypothesis (26) that simple receptive fields belong to a class of linear spatial filters analogous to those described by Gabor (16) and referred to here as 2D Gabor filters.

2. In the space domain, we found 2D Gabor filters that fit the 2D spatial response profile of each simple cell in the least-squared error sense (with a simplex algorithm), and we show that the residual error is devoid of spatial structure and statistically indistinguishable from random error.

3. Although a rigorous statistical approach was not possible with our spectral data, we also found a Gabor function that fit the 2D spectral response profile of each simple cell and observed that the residual errors are everywhere small and unstructured.

4. As an assay of spatial linearity in two dimensions, on which the applicability of Gabor theory is dependent, we compare the filter parameters estimated from the independent 2D spatial and spectral measurements described above. Estimates of most parameters from the two domains are highly correlated, indicating that assumptions about spatial linearity are valid.

5. Finally, we show that the functional form of the 2D Gabor filter provides a concise mathematical expression, which incorporates the important spatial characteristics of simple receptive fields demonstrated in the previous two reports. Prominent here are 1) Cartesian separable spatial response profiles, 2) spatial receptive fields with staggered

subregion placement, 3) Cartesian separable spectral response profiles, 4) spectral response profiles with axes of symmetry not including the origin, and 5) the uniform distribution of spatial phase angles.

6. We conclude that the Gabor function provides a useful and reasonably accurate description of most spatial aspects of simple receptive fields. Thus it seems that an optimal strategy has evolved for sampling images simultaneously in the 2D spatial and spatial frequency domains.

## INTRODUCTION

Our concepts of visual information processing in mammalian striate cortex have been dominated by two major classes of experimental observation. First, the receptive fields of striate neurons are well defined, restricted to small regions of space, and in the case of simple cells, highly structured (17). Second, striate neurons respond to narrow ranges of stimulus orientation (17) and spatial frequency (6), the angular and radial polar coordinates of the two-dimensional (2D) spatial frequency domain. These observations have given rise to divergent theories according to which striate cells have been considered either as feature detectors (27, 28), or as spatial frequency filters (9, 25).

These two descriptions are in fact compatible. Once a mechanism is found to have linear response properties, filter theory becomes applicable, and the debate reduces to the question of whether the mechanism is more sharply tuned in the space domain or the spatial frequency domain (2, 31). The resolution (sharpness of tuning) of a filter in either domain is reciprocally related to its resolu-

tion in the other. For instance, sharpening resolution in the space domain sacrifices resolution in the spatial frequency domain. Gabor (16) described a unique family of linear filters that behave optimally under this uncertainty principle in the sense that their simultaneous resolution in the two domains is maximal. Along one axis, the spatial structure of simple receptive fields bears a remarkable resemblance to Gabor's family of linear filters (26), suggesting that simple receptive fields provide the best possible simultaneous description of the spatial position and spectral content of visual stimuli.

Simple receptive fields, like retinal images themselves, are 2D in space. If Gabor's optimization principle is to apply to spatial vision, it must first be generalized to 2D. Daugman (7) noted that in 2D form, resolution for the two coordinates of spatial position enters into an uncertainty relation with resolution for the two coordinates of the 2D spatial frequency domain (interpretable as orientation and spatial frequency), and that the optimal solution to this joint 2D uncertainty problem embraces a family of functions consisting of bivariate elliptic Gaussians modulated by sinusoidal plane waves. Following Daugman, we refer to these functions as 2D Gabor filters.

This paper describes our efforts to test the hypothesis that simple receptive fields in cat striate cortex are linear filters having the functional form of 2D Gabor filters. Verification of this hypothesis would result in a mathematical scheme unifying key properties of simple receptive fields: periodicity along the width axis, summation along the length axis, spatial frequency tuning, and orientation tuning. Like the well-known difference-of-Gaussians model of retinal ganglion cell receptive fields (35), the 2D Gabor filter model would provide a single expression describing the structure of simple cell receptive fields in two spatial dimensions. It would suggest that the optimization principle on which the 2D Gabor filter is based can be applied to problems in visual information processing, and it would indicate that an efficient strategy is used to represent images in the striate cortex. Because these filters optimize simultaneous resolution in space and spatial frequency, they would minimize the number of filters (cells) required to represent

these two aspects of the information content of images.

## METHODS

To fairly evaluate the 2D Gabor filter hypothesis, we must allow for its general form (7). The optimality constraints permit an elliptic Gaussian of arbitrary orientation, spatial variances, and spatial location, modulated by a sinusoid of arbitrary spatial frequency, orientation, and spatial phase angle. In the discussion that follows, we make explicit the forms we may expect to observe under this hypothesis.

### *Observable form of the 2D Gabor filter in the space domain*

A 2D elliptic Gaussian centered on the origin of a Cartesian coordinate system, with major and minor axes parallel to the coordinate axes can be written

$$w(x, y) = \exp[-1/2(x^2/a^2 + y^2/b^2)]$$

where  $a^2$  is variance in the  $x$  direction and  $b^2$  is variance in the  $y$  direction. The elliptic Gaussian can be centered at any desired spatial location by translating ( $t$ ) coordinates through the desired spatial offsets  $x_0$  and  $y_0$

$$x_t = x - x_0$$

$$y_t = y - y_0$$

The major and minor axes of the Gaussian ( $g$ ) can be aligned in an arbitrary orientation by a rotation of coordinates through a counterclockwise angle  $A$  using

$$x_g = x_t \cos(A) - y_t \sin(A)$$

$$y_g = x_t \sin(A) + y_t \cos(A)$$

Using these substitutions we can write an equation for an elliptic Gaussian of arbitrary orientation centered at an arbitrary spatial coordinate as

$$w(x, y) = \exp[-1/2(x_g^2/a^2 + y_g^2/b^2)]$$

This function has five free parameters:  $a^2$  and  $b^2$  are the spatial variances in the  $x_g$  and  $y_g$  directions, respectively;  $x_0$  and  $y_0$  are the  $x$  and  $y$  locations of the center with respect to the original coordinate system;  $A$  specifies the rotation of the coordinates on which the Gaussian is given with respect to the original coordinate system. The parameters  $x_0$ ,  $y_0$ , and  $A$  are implicit from the substitutions. Figure 1B illustrates an elliptic Gaussian.

A 2D sinusoidal plane wave can be written

$$m(x, y) = \exp[-2\pi i(U_0x + V_0y)]$$

where  $U_0$  and  $V_0$  are spatial frequencies (in cpd) in

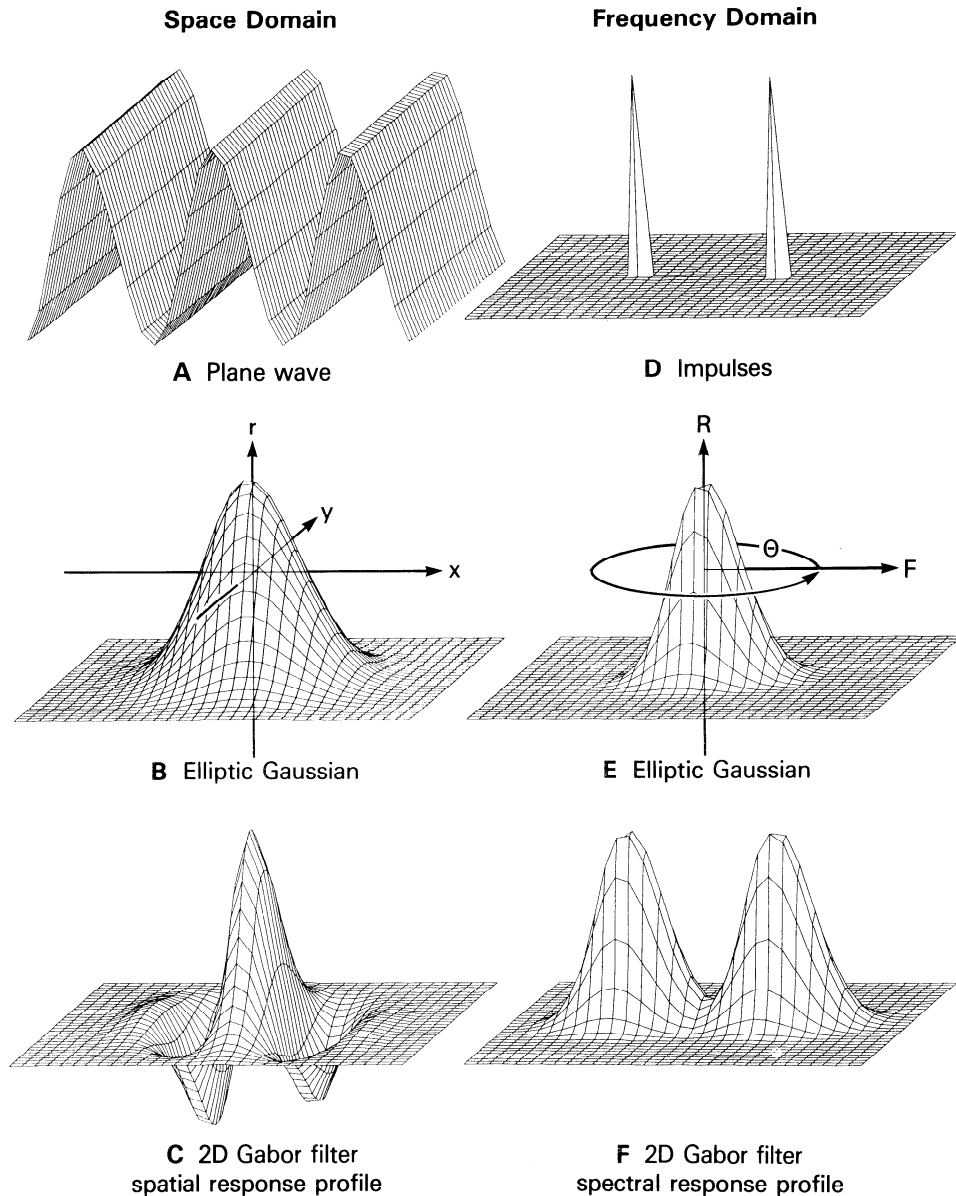


FIG. 1. Structure of two-dimensional (2D) Gabor filters in the space (*left*) and spatial frequency (*right*) domains. In the space domain, a 2D Gabor filter (*C*) can be described as the product of a sinusoidal plane wave (*A*) and a bivariate elliptic Gaussian (*B*). In the spatial frequency domain, a 2D Gabor filter (*F*) can be described as the convolution of a pair of impulses at a specific frequency (*D*) and an elliptic Gaussian (*E*). Graphs in the left- and right-hand columns are of Fourier transform pairs. The coordinates of the 2D space domain are illustrated in *B*. The surface *r* is a function of the two Cartesian variables *x* and *y*. The coordinates of the 2D spatial frequency domain are illustrated in *E*. The surface *R* can be thought of as a function of the polar variables spatial frequency (the radial axis *F*) and orientation (the angular axis *Θ*). In *B* and *E*, the axes have been drawn above the base plane for clarity.

the *x* and *y* directions, respectively. Using Euler's formula, this can be written

$$m(x, y) = \cos [-2\pi(U_0x + V_0y)] \\ + i \sin [-2\pi(U_0x + V_0y)]$$

The optimality of the 2D Gabor filter applies only to the filter in its complex form. In an experiment we can observe only real signals (here, the cosine term). As before, there is no unique property of the coordinate system on which we collect

our data, and we can choose some other origin for the modulation term. It should be noted that the origin of coordinates for the modulation term is quite independent of that for the elliptic Gaussian term. In particular, we can translate our coordinate system by  $x_m$  and  $y_m$

$$m(x, y) = \cos \{-2\pi[U_0(x - x_m) + V_0(y - y_m)]\}$$

and by rearranging

$$m(x, y) = \cos \{-2\pi[U_0x + V_0y - (U_0x_m + V_0y_m)]\}$$

These two constant translation parameters may be concatenated, giving

$$m(x, y) = \cos [-2\pi(U_0x + V_0y) - P]$$

where  $P = (U_0x_m + V_0y_m)$ .

If  $x_m$  and  $y_m$  are chosen so as to give a displacement from the center of the elliptic Gaussian, the parameter  $P$  is naturally interpreted as the relative spatial phase angle of the modulation term. Figure 1A illustrates a sinusoidal plane wave.

The 2D Gabor filter can now be written as the product of an elliptic Gaussian and a sinusoidal plane wave (see Fig. 1C).

$$\begin{aligned} g(x, y) &= K \exp[-1/2(x_g^2/a^2 + y_g^2/b^2)] \\ &\quad \times \cos [-2\pi(U_0x + V_0y) - P] \end{aligned}$$

This equation gives the real (observable) part of a generalized 2D Gabor filter. It is essentially equivalent to the form given by Daugman (7), except in the expression of the decay parameters  $a$  and  $b$ , which he writes in a form reciprocal to the one given here. The scale factor  $K$  is included to permit Gabor filters of any amplitude. This is necessary so that in the curve fitting procedure described below, a best-fitting Gabor filter could be found for data which, although normalized to a peak amplitude of 1.0, were corrupted by noise.

Of course, the modulation term can be expressed in either the Cartesian coordinates  $U_0$  and  $V_0$  as above, or in polar form using the trigonometric relationships

$$F_0 = (U_0^2 + V_0^2)^{1/2}$$

$$\Theta_0 = \arctan(V_0/U_0)$$

The parameters  $F_0$  and  $\Theta_0$  are, respectively, the spatial frequency of the modulation and its orientation.

Thus the 2D Gabor filter functional form we require has nine free parameters. Three of them specify coordinate system conversions (the  $x$  and  $y$  translations and the Gaussian rotation) and can be ignored once they have been found. One of them (amplitude) specifies a scale factor that must be included to allow for noise in the experiment, but which can also be safely ignored once found. The remaining five "essential" parameters (variances along the major and minor axes, spatial fre-

quency, relative orientation, and relative phase) fully characterize the 2D Gabor filter in its most general form.

#### *Observable form in the frequency domain*

In the 2D spatial frequency domain, we must allow for the same variations in filter structure as we allow for in the space domain. There is a further complication, however. In experiments, we can only observe the relative attenuations in amplitude that are imposed on the input sinusoids. To describe this limitation, we say that we measure the amplitude spectrum of the system transfer function. Therefore, we must find the amplitude spectrum of a generalized 2D Gabor filter.

Through the use of Euler's formula, the modulation term can be written

$$\begin{aligned} m(x, y) &= \frac{1}{2}\{\exp[2\pi i(U_0x + V_0y - P)] \\ &\quad + \exp[-2\pi i(U_0x + V_0y - P)]\} \end{aligned}$$

and its 2D Fourier transform is

$$M(U, V) = \exp(-iP)d(U_0, V_0) + \exp(-iP)d(-U_0, -V_0)$$

where  $d$  is a delta function (see Fig. 1D).

The 2D Fourier transform of the elliptic Gaussian term is (see Fig. 1E).

$$W(U, V) = \exp(U_g^2a^2 + V_g^2b^2)$$

The convolution of these last two expressions gives the complex spectrum

$$\begin{aligned} G(U, V) &= \exp(-iP)\exp[-\pi(U_g^2a^2 + V_g^2b^2)] \\ &\quad + \exp(iP)\exp[-\pi(-U_g^2a^2 - V_g^2b^2)] \end{aligned}$$

This expression has six free parameters.  $U_g$  and  $V_g$  both contain two constant translation parameters  $U_0$  and  $V_0$ , which specify the locations of the Gaussian with respect to the origin and a rotation parameter  $A$ , which gives the orientation of the principal axes.  $P$  is the relative spatial phase angle,  $a$  and  $b$  the lengths of the Gaussian principal axes in the  $U_g$  and  $V_g$  directions, respectively.

The amplitude spectrum is given by the square root of the sum of the real and imaginary parts squared. Let  $G_+$  and  $G_-$  denote the two origin-symmetric elliptic Gaussians parts of the previous equation. The complex spectrum may then be written as

$$\begin{aligned} G(U, V) &= \exp(-iP)G_+ + \exp(iP)G_- \\ &= G_+[\cos(P) - i\sin(P)] + G_-[\cos(P) + i\sin(P)] \\ &= \cos(P)(G_+ + G_-) + i\sin(P)(G_- - G_+) \end{aligned}$$

The square of the real part is

$$\cos^2(P)(G_+^2 + G_-^2 + 2G_+G_-)$$

The square of the imaginary part is

$$\sin^2(P)(G_+^2 + G_-^2 - 2G_+G_-)$$

Using the identity  $\cos^2(P) + \sin^2(P) = 1$ , and rearranging, we obtain

$$G(U, V) = G_+^2 + G_-^2 + 2G_+G_-[\cos^2(P) - \sin^2(P)]$$

Using the identity  $\cos^2(P) - \sin^2(P) = \cos(2P)$  and taking the square root, we obtain the 2D Gabor filter amplitude spectrum (see Fig. 1F)

$$G(U, V) = K\{G_+^2 + G_-^2 + 2G_+G_-[\cos(2P)]\}^{1/2}$$

which can be expanded using substitutions for  $G_+$  and  $G_-$ . As before, we include an amplitude term to account for the possibility that the data are corrupted by noise. Thus the functional form we require has seven free parameters, most of which are implicit in the above expression. The relative spatial phase angle appears in the final expression as a constant describing the mixture of the two symmetric elliptic Gaussians. This expression is independent of the spatial location of the filter, a consequence of the shift invariance property of Fourier transforms.

#### *Fitting equations to data*

The evaluation of the 2D Gabor filter hypothesis described in the results section requires that we find a 2D Gabor filter which fits the 2D spatial and 2D spectral response profiles of each simple cell in our population. The partial differential expressions that describe the relationship of the error metric (total squared error) to the 2D Gabor filter parameter set are nonlinear in several of the parameters, so it is impossible to solve the resulting system of equations simultaneously. Instead, we chose the simplex algorithm (33) to minimize the squared error between the 2D Gabor filter functional form and the data. This iterative algorithm searches the multidimensional parameter space for a combination that minimizes the error metric.

We make no effort to describe the simplex algorithm in detail. An extensive formal treatment can be found in Papadimitriou and Steiglitz (34). A more readable (but less complete) presentation can be found in Caceci and Cacheris (5). This algorithm has the desirable properties that it does not require taking derivatives, and it is guaranteed not to diverge. There are two important points one must take into account when using this algorithm.

First, one must decide on a termination criterion. The simplex algorithm manipulates a  $N + 1$  dimensional polygon in an  $N$ -dimensional parameter space; the termination criterion specifies how close the vertices must be to one another to declare that a minimum has been found. We set a rather stringent value for proximity. In all cases every corresponding parameter value in all vertices must have been within 0.5% of one another. The average value of the vertices was taken as the solution.

Second, one must avoid getting trapped in local minima on the error hyperplane. To avoid this pitfall, we ran the simplex several (up to 12) times on each data set using three different initialization strategies. First, we ran each simplex on each surface starting with a manually selected parameter set chosen to be as much like the data surface as possible. Second, we ran the simplex five times on each surface using standard starting parameter sets. Third, we ran the simplex up to six times on each surface using the result of the previous run displaced by a random vector in the parameter space as the input to the new run, thus searching the local neighborhood for deeper minima. After running the algorithm many times, we listed the parameter values, along with the squared error, for each run. We always chose the run that resulted in the least overall squared error for further analysis, even though in most cases the results from separate runs were very close to one another (differences appeared most frequently in the 4th significant decimal digit).

## RESULTS

These results are based on 36 2D spatial response profiles obtained from 36 simple cells and 36 2D spectral response profiles obtained from 36 simple cells in the striate cortices of 14 cats. These two populations do not overlap completely: we obtained both 2D spatial and 2D spectral response profiles for 25 cells. These data, and the methods of obtaining them, were described in detail in the preceding papers (19, 20).

#### *Predictions*

We use the 2D Gabor filter model to make three simple, but comprehensive, predictions. First, simple cell 2D spatial response profiles and 2D Gabor filter spatial profiles will be indistinguishable. Second, simple cell 2D spectral response profiles and 2D Gabor filter amplitude spectra will be indistinguishable. Since the 2D Gabor filter model presupposes linear spatial summation in 2D, we also predict that simple receptive fields will satisfy this constraint. If these three predictions are satisfied, we will accept the 2D Gabor filter model of simple receptive fields.

We evaluate all three predictions. First, we derive a statistical test by which we can decide if an individual 2D spatial response profile has the functional form of a 2D Gabor filter and apply the test to the population of 2D spatial response profiles. Second, we compare 2D spectral response profiles to 2D

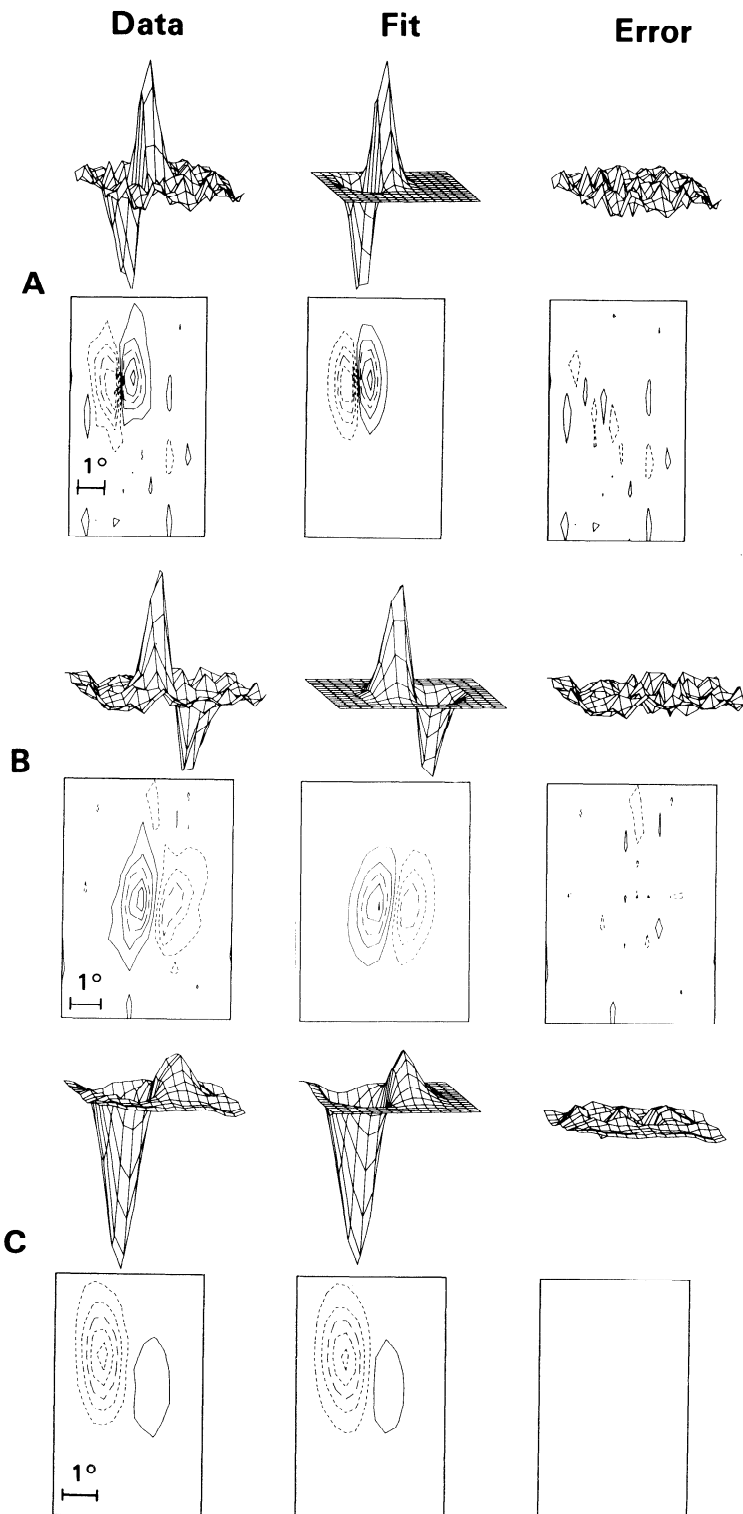
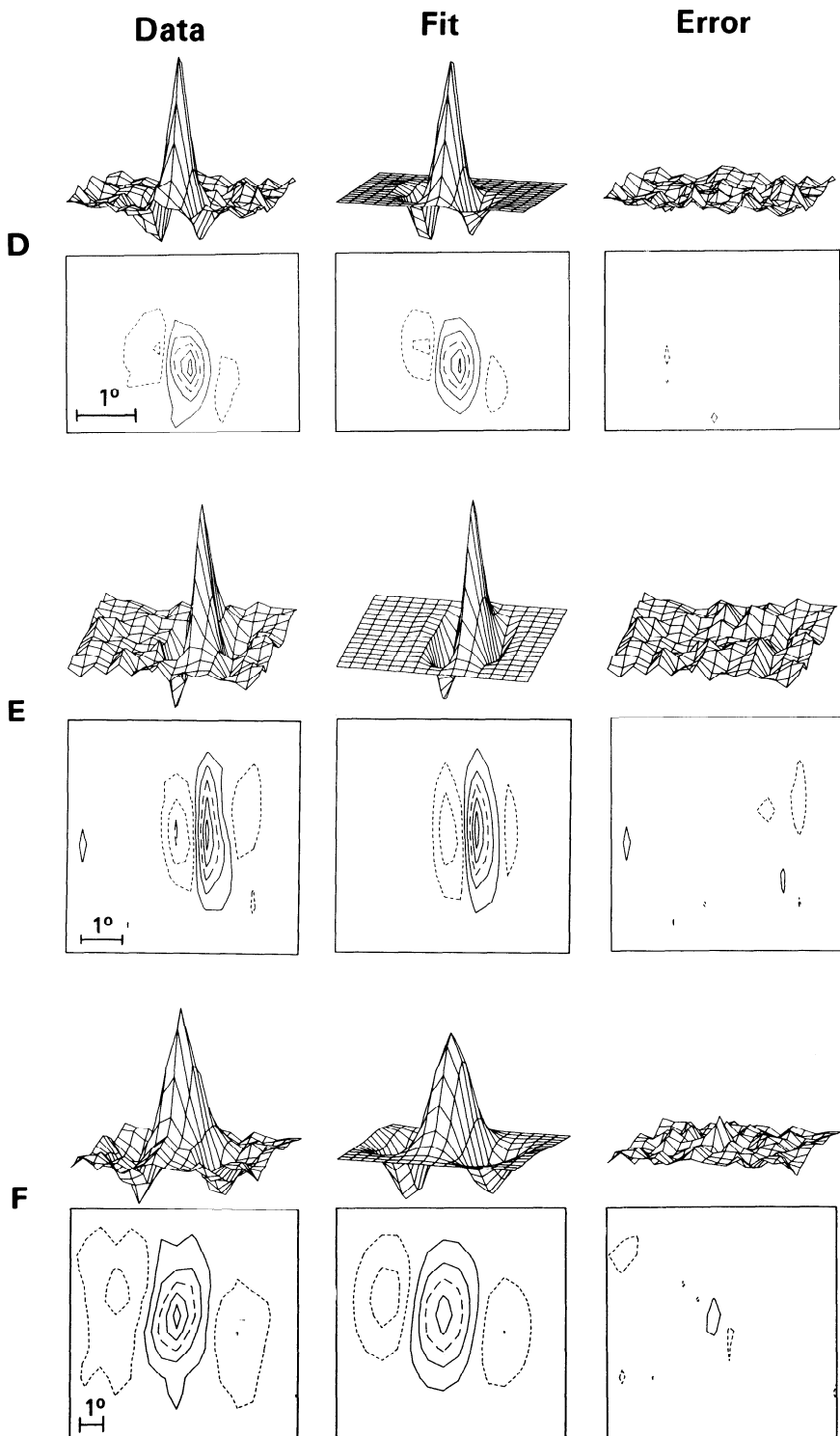
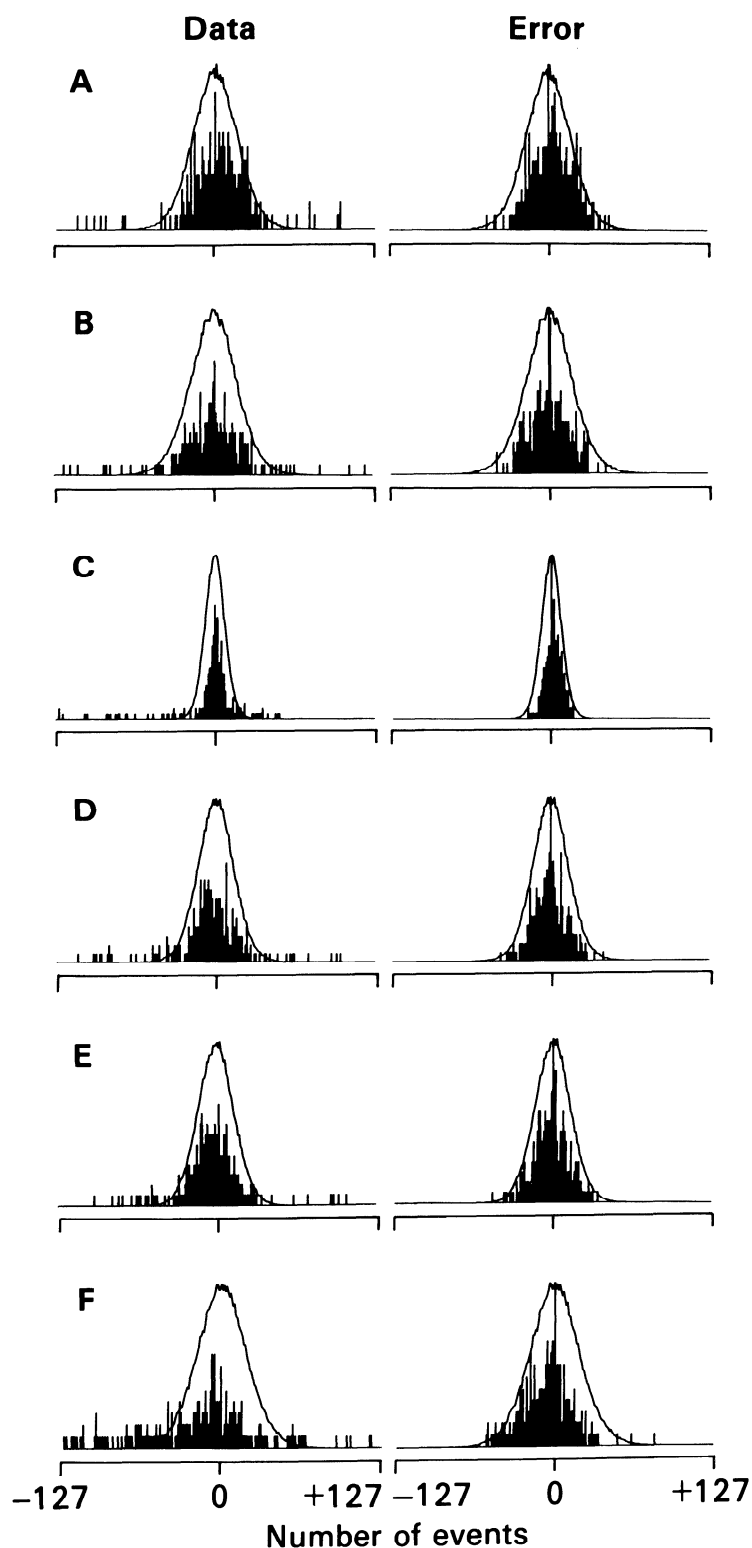


FIG. 2. The two-dimensional (2D) Gabor filter fits simple cell 2D spatial response profiles. Each part of this figure illustrates a 2D spatial response profile, the corresponding least-squared error best-fitting 2D Gabor filter, and the residual error, that function of space which remains after the 2D Gabor filter has been subtracted from the data.

FIG. 2, *cont.*

The 2D Gabor filter describes all of the main features of 2D spatial response profiles. *A*: an odd-symmetric profile in which the 2 subregions are slightly staggered. *B*: a profile close to odd symmetry. *C*: an asymmetric profile. *D* and *F*: 2 profiles close to even symmetry, with staggered subregions. *E*: a Cartesian separable profile.



Gabor filter amplitude spectra in a somewhat less formal environment. Finally, we assess the 2D spatial response linearity of the population of simple receptive fields by comparing the 2D Gabor filter parameter estimates obtained from the space and spatial frequency domains. This last effort is necessary despite prior demonstrations that simple cells linearly combine inputs distributed across their width axes (2, 31), since linearity of spatial summation in 2D does not automatically follow.

### *2D spatial response profiles and 2D Gabor filters*

To determine if simple cell 2D spatial response profiles have the functional form of 2D Gabor filters we assume that the observed profiles  $r(x, y)$  consist of a 2D Gabor filter  $g(x, y)$ , some other deterministic function of 2D space  $h(x, y)$ , and additive Gaussian noise of zero mean and some computable variance  $\sigma_0^2$

$$r(x, y) = g(x, y) + h(x, y) + e \sim N(0, \sigma_0^2)$$

then

$$r(x, y) - g(x, y) = h(x, y) + e \sim N(0, \sigma_0^2)$$

We call the expression on the left the residual error: that function of space in the observed response which cannot be described by the 2D Gabor filter. If  $h(x, y) = 0$ , we can expect

$$r(x, y) - g(x, y) = e \sim N(0, \sigma_0^2)$$

That is, the difference between the observed 2D spatial response profile and some yet to be determined 2D Gabor filter is normally distributed with zero mean and some given variance. If it is not, we can reject the 2D Gabor filter model. This leads to formulable hypotheses

$$H_0: \sigma_1^2 \leq \sigma_0^2$$

$$H_1: \sigma_1^2 > \sigma_0^2$$

where  $\sigma_1^2$  is the variance of the residual error, and  $\sigma_0^2$  is the variance of the noise. That is, if the 2D Gabor filter does not account for all

the variation in the data except that due to random error, we must conclude that  $h(x, y) \neq 0$ , and there is some systematic deviation in the observed 2D spatial response profiles from the template laid down by the 2D Gabor filter functional form. To implement this test we must find the expected variance of the noise, find a 2D Gabor filter that has a fair chance of describing the data, compute the variance of the residual error, and compare this variance to the variance of the noise.

To find the expected variance of the noise, we computed 391 reverse correlations beginning with temporal intervals of 19 stimulus durations (typically 950 ms) and working toward longer intervals. This computation provided 100,096 samples of noise (256 from each temporal interval) from each experiment. Because receptive fields are found within a narrow temporal interval close to the time spikes occurred (19), these samples are devoid of any signal; they represent the expected behavior of the experiment in the absence of a receptive field. The surface that results is devoid of structure and was characterized statistically by producing a histogram (as the solid lines in Fig. 3) showing the number of occurrences of each noise value in the surface. The variance of this amplitude distribution was taken as the variance of the noise.

We used the simplex algorithm to find the 2D Gabor filter that best fit the 2D spatial response profiles in the least-squared error sense. The residual error is simply the point-for-point difference between the data and the fit over the grid surface on which stimuli were presented. Figure 2 illustrates six 2D spatial response profiles, the corresponding 2D Gabor filters, and the residual error in each case. In each example, the 2D Gabor filter describes the profile well.

All of the observed variability in 2D spatial response profiles described qualitatively in the first paper of this series can be described quantitatively using the parameters of the

FIG. 3. Amplitude histograms for raw data, error, and noise. Each part of this figure (A-F) corresponds to A-F of Fig. 2. On the left, an amplitude histogram for the raw data is shown (the incidence of response values over the 256 points in the difference correlograms). The amplitude histogram on the right was computed after the best-fitting Gabor function was subtracted from the correlogram (the residual error). On both the left and right, the amplitude distribution of the noise (computed by repeating the reverse correlation well outside the temporal window in which the cell responds) is presented as a smooth curve for comparison. The variance of the residual error distribution (unlike the data) is not significantly different from the variance of the noise.

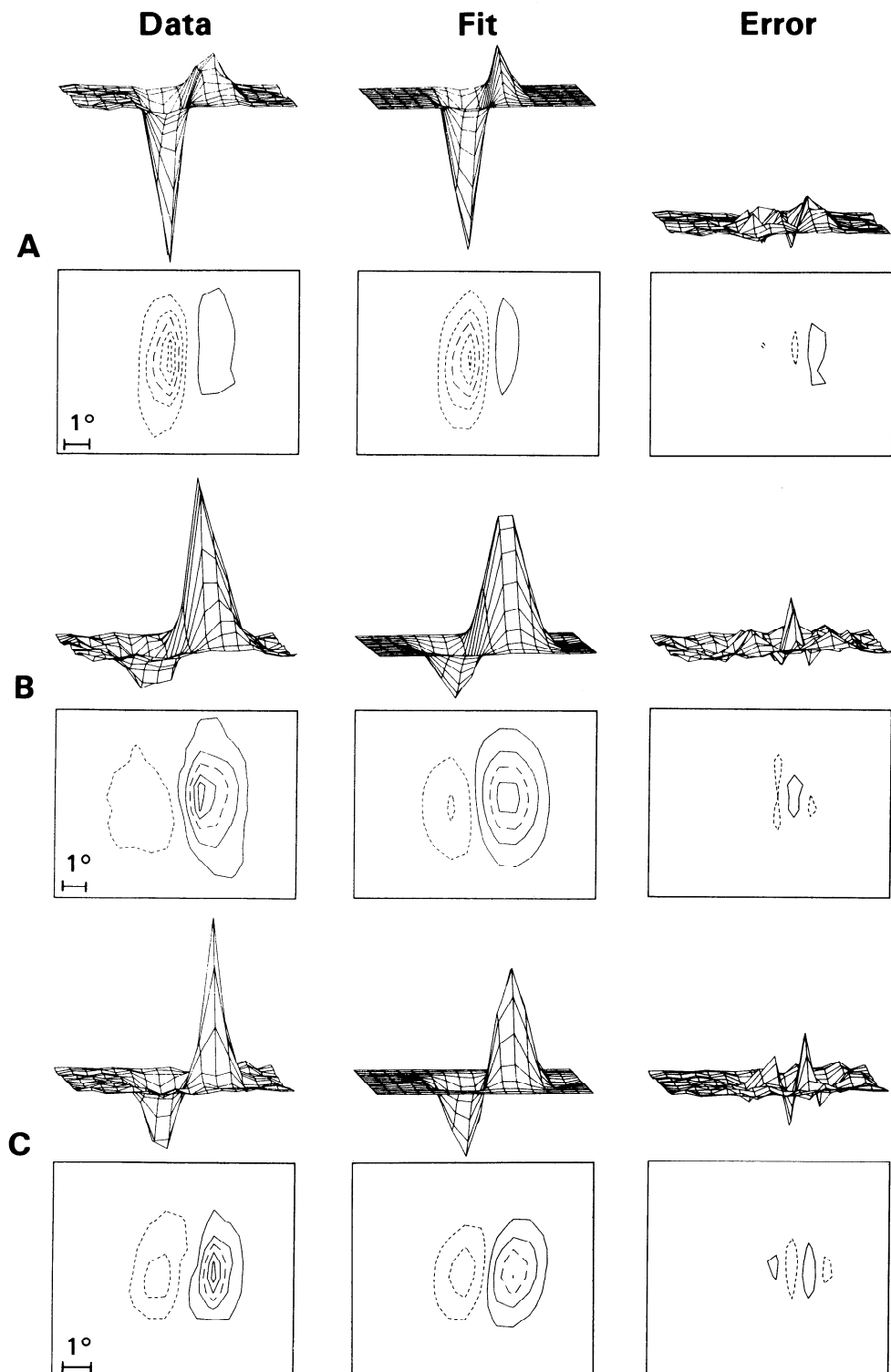


FIG. 4. Only 3 two-dimensional (2D) spatial response profiles of the 36 examined were significantly different from 2D Gabor filters. Each of the residual error surfaces contained some systematic structure.

2D Gabor filter. Figure 2, A and B, illustrates profiles in odd symmetry and near odd symmetry, respectively; Fig. 2C illustrates a profile that is quite asymmetric. Figure 2E illustrates a Cartesian separable profile; Fig. 2, D and F, illustrates profiles that are not Cartesian separable.

The residual error surfaces in Fig. 2 demonstrate that most of the variation in the data is accounted for by a 2D Gabor filter. The residual variation appears small and spatially unstructured. In 33 of the 36 2D spatial response profiles we collected, 2D autocorrelation functions of the residual error revealed no systematic 2D structure.

We may now compare the variance of the residual error with the variance of the noise. Figure 3 illustrates amplitude histograms of the same data illustrated in Fig. 2. The solid curves in each part represent the distribution of amplitudes expected in the absence of a receptive field (see METHODS). The solid histograms in the column labeled ERROR represent the distribution of amplitudes found in the residual error surfaces. In each case, it is apparent that the error histogram is reasonably well contained within the noise histogram.

For comparison, Fig. 3 also illustrates amplitude distributions taken from the original data (in the column labeled DATA). These histograms are quite obviously not contained by the noise histograms, which allows us to make the trivial conclusion that there was a signal in the data. Because the error histograms were contained, we make a more significant conclusion: all of the variation in the original data except that due to random error can be described by a 2D Gabor filter.

The statistic

$$Z = [2x_n^2]^{1/2} - [2(n-1)]^{1/2}$$

was derived from the *f* distribution which becomes chi-square ( $\chi_n^2$ ) when the degrees of freedom ( $n$ ) in the denominator is large (because we have so many data points). It is distributed according to the standard normal distribution (15, 29). We computed  $Z$  for each residual error histogram in our population. The decision criterion was that for  $Z > 1.65$  we would reject the null hypothesis ( $P < 0.10$ ).

In 33 out of the 36 cells the statistic  $Z$  failed to reach significance. Thus in these cases we do not have enough evidence to re-

ject the 2D Gabor filter hypothesis, so we must accept it. We note that with a probability of  $P < 0.1$  there is ample opportunity to reject the hypothesis. Indeed, out of 36 cases we would expect 3.6 cases to be rejected by this test, even if the null hypothesis were always true. Because we only reject 3 of the 36 cases, we are within the bounds established by our expectations.

The three cases that did not pass the statistical test are illustrated in Fig. 4. These 2D spatial response profiles have in common that a subregion is more or less sharply peaked than we expect from the 2D Gabor filter model. This shows up as periodic structure in the residual error, and many significant nonzero elements in its 2D autocorrelation function (not illustrated). We can offer no explanation as to why the 2D Gabor filter does not fit these data.

#### *2D spectral response profiles and 2D Gabor filters*

We turn now to the second prediction, that simple cell 2D spectral response profiles will be indistinguishable from 2D Gabor filter amplitude spectra. Ideally, one would like to employ a statistical decision criterion to each profile, but two factors prevent it. First, because simple cell response variability increases with response amplitude (8, 36, 37), it is impossible to assign a single expected error distribution to the entire data set. Second, the data were not collected with uniform sampling intervals, which impedes the calculation of a 2D autocorrelation function. Overcoming these two obstacles would have required rebuilding much of the laboratory, so we settled for a partial analysis. The simplex algorithm was used to find the 2D Gabor filter amplitude spectrum that best fit the data in the least-squared error sense, the residual error was calculated, and the quality of fit was evaluated by eye through an examination of the residual error surfaces.

Figure 5 illustrates six examples of 2D spectral response profiles, the corresponding best-fitting 2D Gabor filter amplitude spectra, and the residual error. In each example, the 2D Gabor filter fits the data remarkably well. All of the features of the 2D spectral response profiles itemized in the previous paper are accounted for by 2D Gabor filters, including nonradial elongation (20).

In the residual error surfaces, one can see

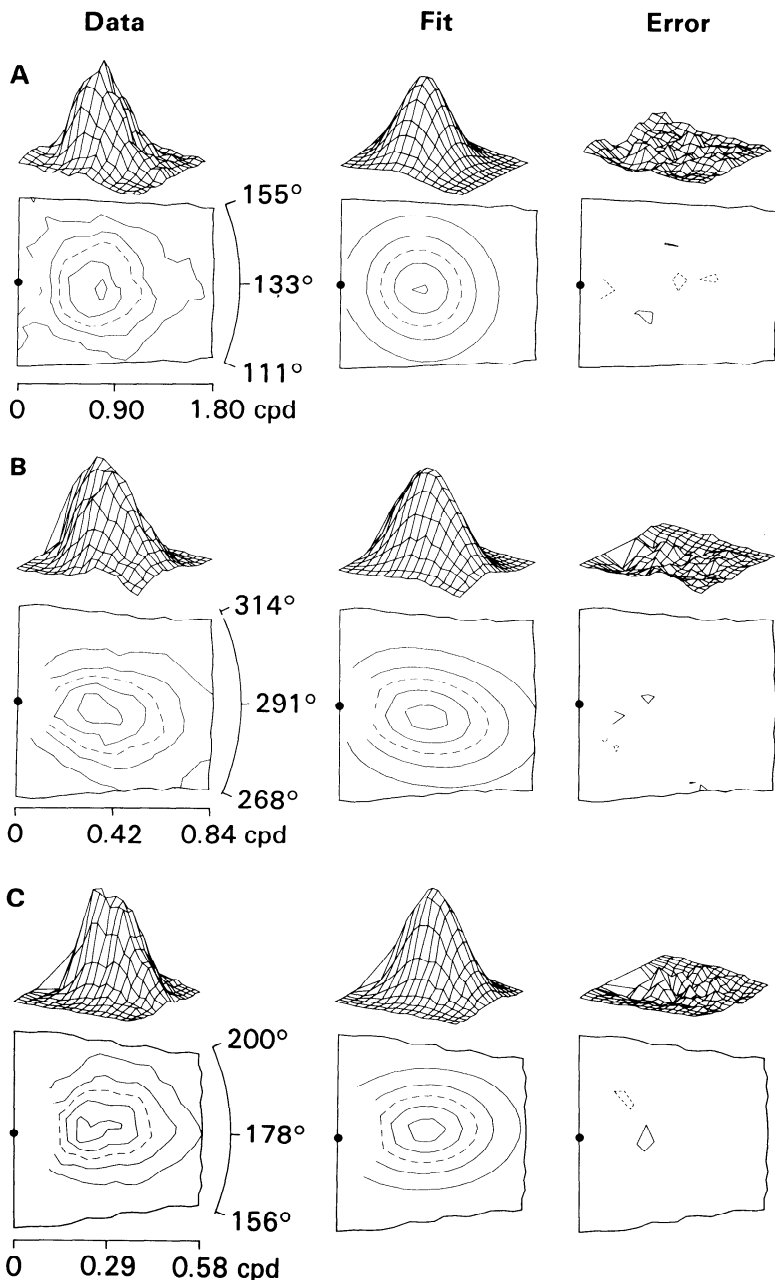


FIG. 5. The two-dimensional (2D) Gabor filter fits simple cell 2D spectral response profiles. Each part of this figure illustrates a 2D spectral response profile, the corresponding least-squared error best-fitting 2D Gabor filter amplitude spectrum, and the residual error. The 2D Gabor filter accommodates all of the main features of 2D spectral response profiles. *A*: a circularly symmetric profile. *B* and *C*: radially elongated profiles. *D–F*: nonradially elongated profiles. The nonradial elongation in *D* can best be detected in the fitted function.

in each case that most of the variability in the data is accounted for by the 2D Gabor filter. The variation that remains is unlike the residual variation in the space domain experi-

ment. Here, the amplitudes of the residual errors are small near the edges of the grids (where there is no response) and increase as one moves toward the centers of the grids

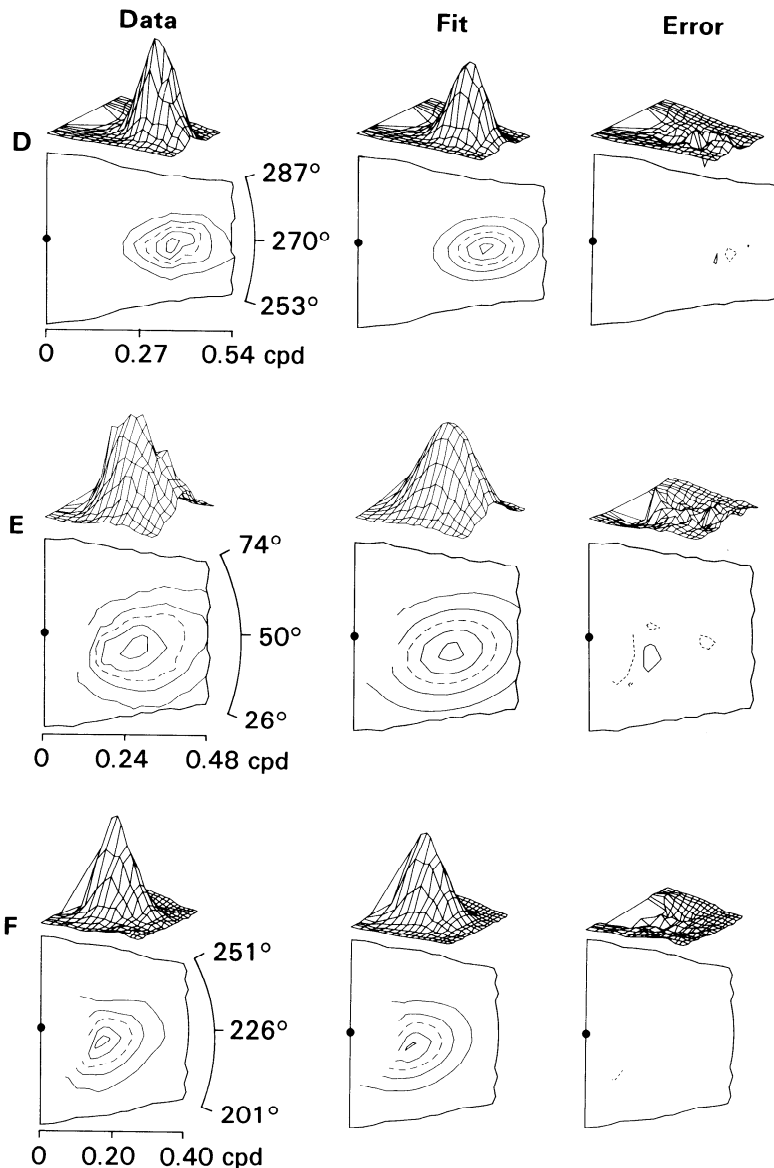


FIG. 5. (continued)

(close to the largest response). There is, however, no tendency for the residual errors to be preferentially above or below zero.

Because we had no objective criterion for determining if the 2D Gabor filter fit the data, we scrutinized all of the residual error surfaces for evidence of systematic deviations. Figure 6 illustrates the two profiles which, in our opinions, deviated from the best-fitting 2D Gabor filter. The profile illustrated in Fig. 6A contained a skew that was unaccounted for; the data surface leans

slightly toward low spatial frequencies, whereas the fitted 2D Gabor filter is radially symmetric about its peak. As a consequence, there is a radial ripple in the residual error surface. The data in Fig. 6B had nonelliptical isoresponse-amplitude contours. Consequently, there are two lateral peaks and a central trough in the residual error surface.

The two profiles in Fig. 6 were the only two examples of systematic deviation we could find in the population of 36. Therefore, we conclude that the 2D Gabor filter

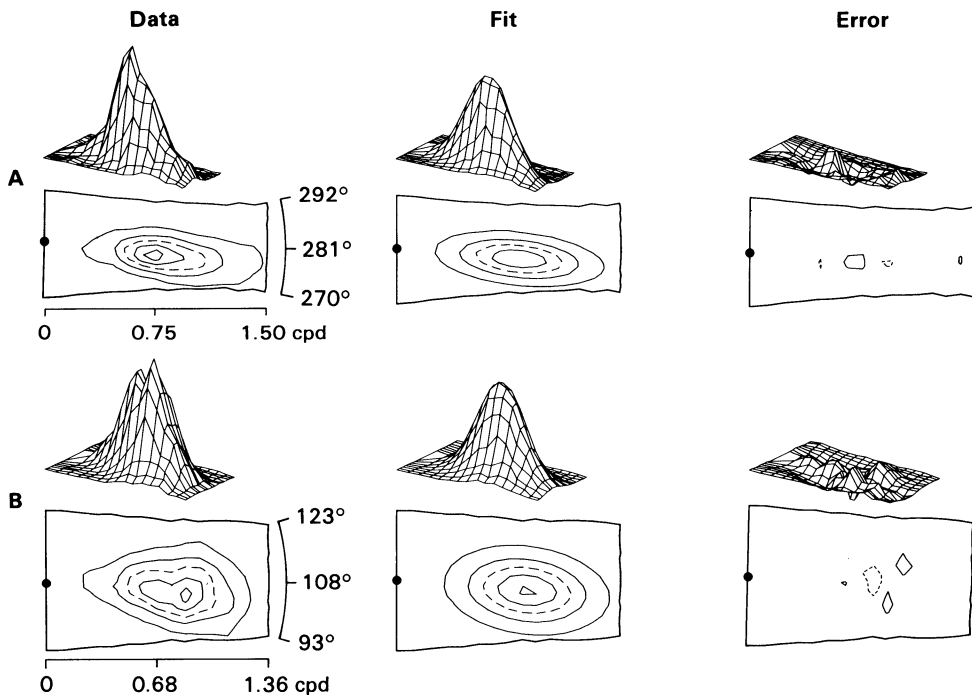


FIG. 6. Careful examination of the residual error surfaces revealed that only 2 spectral response profiles out of 36 were not well described by two-dimensional (2D) Gabor filters. *A*: the residual error surface exhibits some radial ripple; the data were skewed slightly more than the 2D Gabor filter. *B*: the residual error surfaces exhibits a cluster of 4 extrema; isoresponse-amplitude contours around the data were not quite elliptical.

provides an excellent model of simple cell 2D spectral response profiles.

#### *Response linearity*

In the results presented above, the 2D Gabor filter was demonstrated to accurately describe both the 2D spatial response profiles and the 2D spectral response profiles of simple cells. These demonstrations were separate, however, and no attempt was made to determine if the filter that described the space domain data was the same as the filter that described the frequency domain data. If a simple receptive field exhibits response linearity over two spatial dimensions, and if 2D Gabor filters accurately describe its responses in both the space domain and the spatial frequency domain, then the space domain Gabor filter and the frequency domain Gabor filter must be Fourier transform pairs (they are the same filter).

This leads to a simple evaluation of 2D spatial response linearity: if the 2D Gabor

filter describing the space domain data and the 2D Gabor filter describing the frequency domain data have the same parameters, then the receptive field combines spatially distributed inputs linearly.

We compared the parameter sets for all the profile pairs in our sample and found that in no cases were all of the parameters identical. In fact, it was rare for even a single pair of parameters from the space and spatial frequency domains to be the same beyond two decimal digits. This result is unsurprising, though, for several reasons. First, the measurements represent an estimate of the true response profile in either domain. Second, fitting parameters to the data represents another level of estimation. In the discussion that follows, it is worthwhile to remember that we are comparing estimates of estimates.

Although we know the parameters of the best-fitting 2D Gabor filters in both domains for 25 cells, we cannot implement a simple test on any of them in any meaningful way, since it was not possible to generate confi-

TABLE 1. 2D Gabor filter parameter estimates obtained from space and spatial frequency domains for 25 cells

Cell	Space Domain Estimates						Frequency Domain Estimates					
	Wavevector frequency, cycles/deg	Wavevector orientation, deg	Effective width, deg	Effective length, deg	Relative orientation, deg	Relative phase, deg	Wavevector frequency, cycles/deg	Wavevector orientation, deg	Effective width, deg	Effective length, deg	Relative orientation, deg	Relative phase, deg
0608	0.39	22	1.29	1.67	4	90	0.51	22	0.35	0.31	2	69
0309	0.49	166	1.11	2.22	8	11	0.81	166	0.74	0.45	8	85
0409	0.47	167	1.26	1.54	-22	6	0.71	167	0.50	0.44	-13	2
0809	0.51	113	1.01	1.60	-8	51	0.79	113	0.64	0.54	-11	64
0909	0.28	13	2.16	2.54	26	44	0.35	13	0.48	0.35	41	54
0511	0.63	132	1.23	2.28	-1	7	0.68	129	0.79	0.49	-7	0
0611	0.53	144	0.84	0.90	-4	11	0.74	131	0.85	0.78	-23	61
0711	0.47	137	0.95	1.31	-29	86	0.54	131	0.52	0.34	-43	71
0811	0.70	98	0.86	2.07	5	37	0.83	96	0.68	0.21	1	50
1311	0.42	79	1.32	3.32	11	38	0.35	76	0.44	0.15	3	90
0212	0.30	67	2.26	3.69	4	46	0.35	70	0.50	0.24	1	72
0612	0.29	133	2.30	3.66	-6	81	0.31	131	0.47	0.25	-11	0
0414	0.06	21	2.04	4.47	3	80	0.28	28	0.31	0.16	0	82
0914	0.39	58	0.84	1.60	-2	29	0.59	62	0.64	0.36	-6	45
1014	0.21	124	0.80	3.39	-9	2	0.32	118	1.25	0.29	-1	75
0415	0.56	104	1.03	1.87	6	81	0.80	104	0.60	0.32	3	90
0116	0.19	95	3.70	5.75	27	41	0.19	115	0.24	0.14	6	90
0316	0.20	108	0.94	2.27	3	33	0.25	103	1.12	0.40	-2	90
0218	0.29	105	1.63	2.31	3	47	0.38	103	0.59	0.34	-2	90
0219	0.66	50	0.76	1.34	41	31	0.77	47	1.20	0.81	-22	77
0319	0.05	169	2.71	3.71	-11	54	0.24	168	0.34	0.30	-34	84
0619	0.20	175	2.49	3.05	26	4	0.14	161	0.38	0.27	38	13
0719	0.28	126	1.87	4.00	-10	70	0.30	121	0.49	0.23	-21	24
0122	0.17	33	3.56	5.39	-28	6	0.16	35	0.20	0.13	-27	38
0224	0.14	98	1.60	3.30	-8	67	0.20	102	0.28	0.16	-11	90

The plane-wave parameters are given in terms of spatial frequency (cycles per degree of visual angle) and orientation (degrees counterclockwise from horizontal). The elliptic Gaussian parameters are given as effective width (degrees of visual angle), and effective length (degrees of visual angle). See text for definitions. The relationship of the plane wave and the elliptic Gaussian is described by the relative orientation (degrees counterclockwise from parallel) and relative phase (absolute value in degrees relative to cosine phase).

dence intervals around each estimated parameter. Hence, we cannot compare individual space domain fits to individual frequency domain fits. Instead, we evaluate the response linearity of the population as a whole. If each simple cell is a linear filter in 2D of space, then the behavior of the whole population should follow suit.

We constructed scatter diagrams and computed correlation coefficients using parameter estimates for 2D Gabor filters from both 2D domains for the whole population of cells (see Table 1). These scatter diagrams were arranged so that the distribution of space domain parameters lies along the horizontal axis, and the distribution of frequency domain parameters lies along the vertical axis. Solid lines in each graph represent theoretical predictions. If all simple cells were 2D Gabor filters, if all parameter estimates were perfect, and if all simple cells responded linearly, then all of the symbols in each scatter

diagram would lie precisely along the solid lines.

#### Spatial frequency and orientation

Figure 7 illustrates the estimated modulation parameters spatial frequency and orientation. Parameter estimates made from the space domain data are distributed along the abscissa; those made from the frequency domain data along the ordinate. Estimates of plane wave orientation (Fig. 7B) made from the two domains agree very well: the correlation coefficient is 0.99, and all of the points in the scatter diagram lie very close to the diagonal line of unit slope and zero intercept.

Estimates of plane wave spatial frequency agree less well. They are strongly correlated ( $r = 0.91$ ), but most of the symbols in Fig. 7A lie above the diagonal line. Plane wave spatial frequency is slightly underestimated using space domain data, or slightly overestimated using frequency domain data, or both. We interpret this shift as a systematic bias of

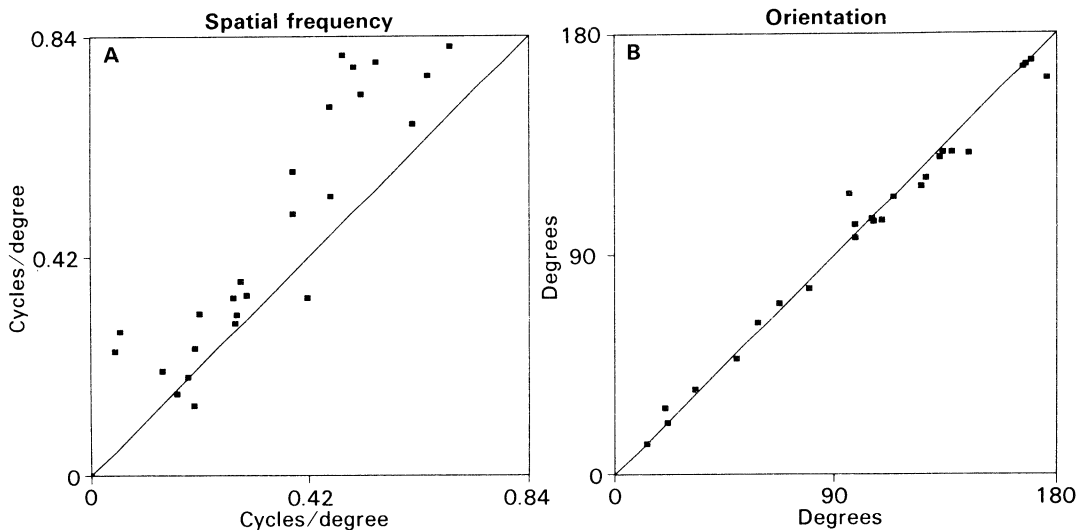


FIG. 7. Parameters of the two-dimensional (2D) Gabor filter plane wave as estimated from 2D spatial and spectral response profiles. *A*: spatial frequency estimates should be identical (*diagonal line*). There is a strong linear relationship ( $r = 0.91$ ), but most of the points lie above the *diagonal line*. This error is probably due to a systematic bias of unknown origin in the estimation procedure. *B*: plane-wave orientation estimates should be identical. For all practical purposes, they are ( $r = 0.99$ ).

unknown origin in the estimation procedures. The average absolute value of the difference between the two estimates is 0.11 cpd.

#### *Relative orientation and relative spatial phase*

The relationships between the plane wave and the elliptic Gaussian terms of the 2D

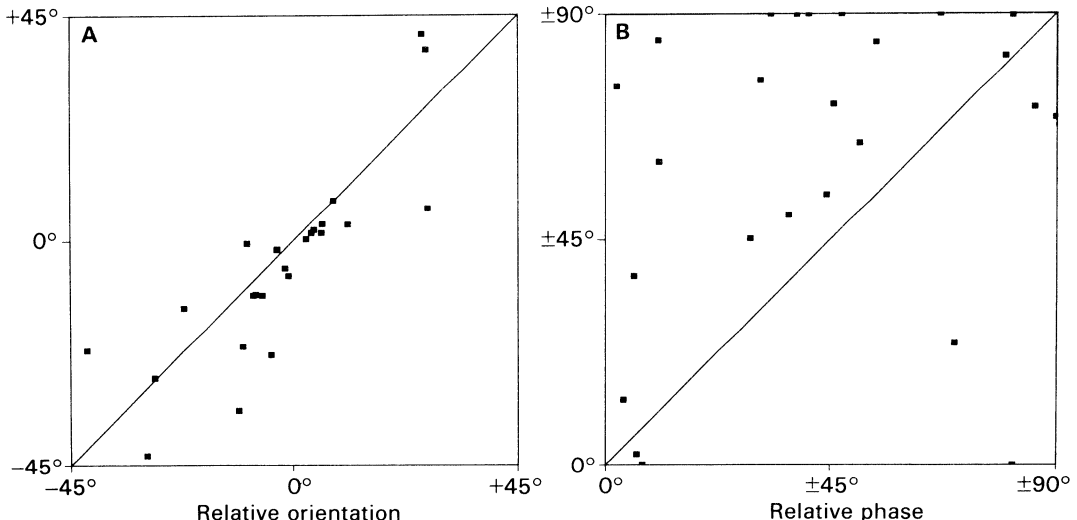


FIG. 8. The relationships between the two-dimensional (2D) Gabor filter plane wave and elliptic Gaussian as estimated from 2D spatial and spectral response profiles. *A*: estimates of relative orientation should be identical (*solid diagonal line*). There is reasonably good correlation between the 2 estimates ( $r = 0.84$ ) and a strong tendency for alignment of the modulation and a principal axis. *B*: estimates of relative spatial phase should be identical, but there is almost no correlation between the 2 estimates ( $r = 0.27$ ). Furthermore, the frequency domain estimates tend toward sine phase, whereas the space domain estimates have no central tendency.

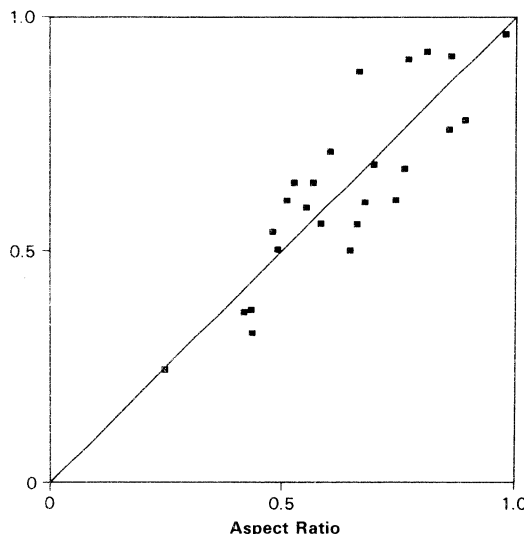


FIG. 9. The shape (aspect ratio) of the two-dimensional (2D) Gabor filter elliptic Gaussian term as estimated from 2D spatial and spectral response profiles should be identical (*solid diagonal line*). There is reasonably good correlation between the 2 estimates ( $r = 0.86$ ), and the points have no tendency to lie above or below the *diagonal line*. The shapes of 2D spatial and spectral response profiles are therefore roughly the same.

Gabor filter are captured by two parameters: relative orientation and relative spatial phase. The estimated differences in orientation between the plane wave and the space domain elliptic Gaussian minor axis (abscissa) and the plane wave and the frequency domain elliptic Gaussian major axis (ordinate) are illustrated in Fig. 8A. There is reasonably close agreement between the two estimates ( $r = 0.84$ ). In particular we note a strong tendency for the relative orientation of the two terms to be zero. In about half (11/25) of the profiles, the plane wave was oriented within  $\pm 10^\circ$  of the appropriate principal axis. For the remainder of the profiles, both the space domain and the frequency domain data yielded an estimated relative orientation  $> 10^\circ$ .

This result provides the quantitative connection between the subregion staggering observed in 2D spatial response profiles (19) and the nonradial elongation observed in 2D spectral response profiles (20). Figures 2F and 5F illustrate 2D spatial and spectral response profiles obtained from the same cell. In the 2D spatial response profile (Fig. 2F)

the subregions are staggered with respect to one another along their long axes; the 2D spectral response profiles (Fig. 5F) exhibits nonradial elongation. The best-fitting 2D Gabor filter profiles estimate a relative orientation of  $-27^\circ$  in both the space domain and the spatial frequency domain. (Most of the estimate pairs do not agree this well, particularly for large values of relative orientation.)

The relative spatial phase between the plane wave and the elliptic Gaussian is illustrated in Fig. 8B. The agreement between the space and frequency domain estimates is particularly poor. The correlation coefficient is only 0.27 (the sign, at least, is correct), 19 of the 25 points lie above the diagonal line, and 6 lie along the top edge of the graph. Thus the frequency domain estimate typically lies closer to sine phase ( $\pm 90^\circ$ ) than the space domain estimate. This lack of correlation arises primarily from the insensitivity of our frequency domain methods to spatial phase (see DISCUSSION).

#### *Shape and size of elliptic Gaussian*

According to the 2D Gabor filter model, the shapes of the fitted elliptic Gaussians in the two domains should be identical, and their sizes should be reciprocal.

The shape of the elliptic Gaussian was determined by taking the ratio of the minor axis to the major axis, giving a dimensionless number in the range 0–1 (the aspect ratio). Figure 9 illustrates the elliptic aspect ratios as estimated from the space and frequency domain data. There is a reasonably strong correlation between the two estimates ( $r = 0.86$ ), and the points show no preference for distribution above or below the diagonal line. There is a tendency for the points to cluster about a value of 0.6; 2D spatial response profiles tend to be nearly twice as long as they are wide, and 2D spectral response profiles twice as wide as they are long. There is no absolutely preferred aspect ratio; the observed values are in the range 0.23 (nearly 5 to 1 elongation) to 0.92 (nearly round). We conclude that the observed shapes of the elliptic Gaussian in the two domains is the same, as expected.

The effective length, width, and size of the elliptic Gaussian can be defined using the lengths of the principal axes. If we let  $a_s$  and  $b_s$  denote the lengths of the minor and major

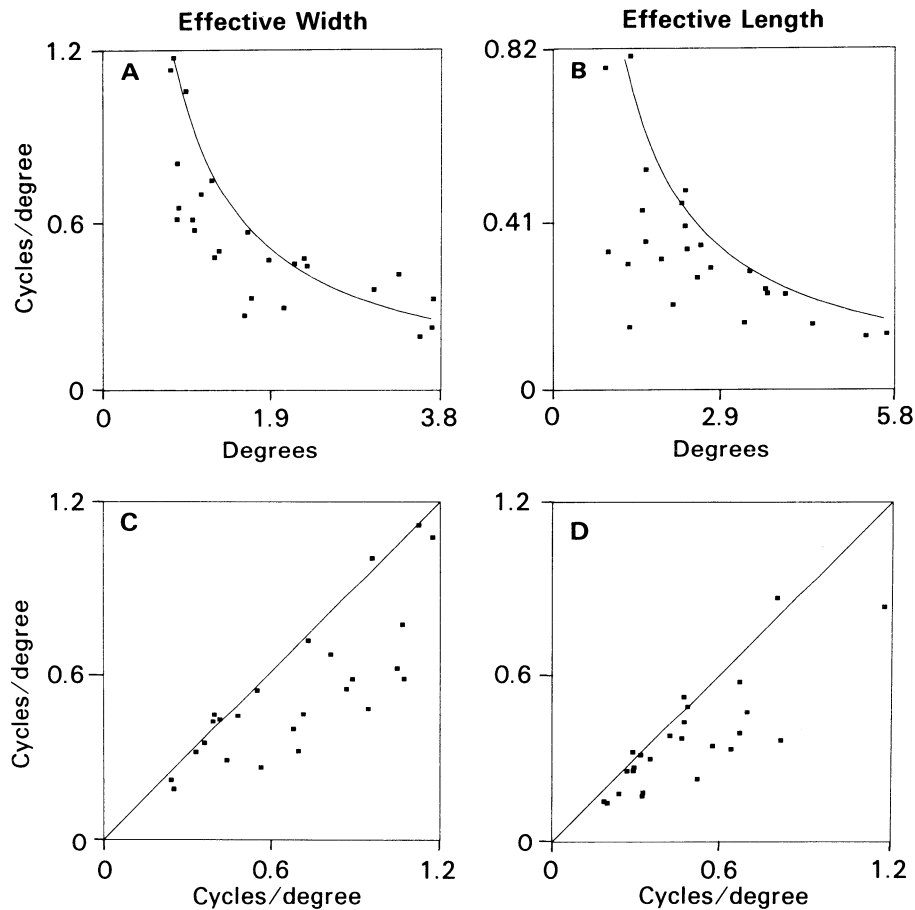


FIG. 10. The sizes (lengths of the major and minor axes) of the two-dimensional (2D) Gabor filter elliptic Gaussian term as estimated from 2D spatial and spectral response profiles should be inverses (*solid hyperbolae*). *A*: estimates of the space domain minor axis and the frequency domain major axis frequently follow this rule (many points lie on or near the *hyperbola*), but some do not (the points lie inside the *hyperbola*). *B*: similar results are obtained for the relationship between the space domain major axis and the frequency domain minor axis. *C* and *D*: estimates of the decay parameters  $a$  and  $b$  should be identical (*solid diagonal lines*). Many of the points lie on or near the *diagonal lines*, but some lie below. The correlation coefficients are 0.80 for *C* and 0.81 for *D*.

axes of the elliptic Gaussian in the space domain, and  $a_f$  and  $b_f$  denote the lengths of the major and minor axes in the frequency domain, then the 2D Gabor filter model predicts

$$\text{effective width: } \pi^{1/2} a_s = 1/\pi^{1/2} a_f$$

$$\text{effective length: } \pi^{1/2} b_s = 1/\pi^{1/2} b_f$$

Consequently,

$$\text{effective area: } \pi a_s b_s = 1/\pi a_f b_f$$

We may thus define the effective width of the elliptic Gaussian in the space domain as

the length of its minor axis times the square root of  $\pi$  (root  $\pi$ ), the effective length as root  $\pi$  times the length of the major axis, and the effective area as  $\pi$  times the lengths of the major and minor axes. The width is typically measured in a direction nearly parallel to the receptive field modulation axis, and the length in a direction perpendicular to the width. Similar definitions are adopted for the spatial frequency domain, where the width is typically measured in a nearly radial direction and the length in a direction perpendicular to the width.

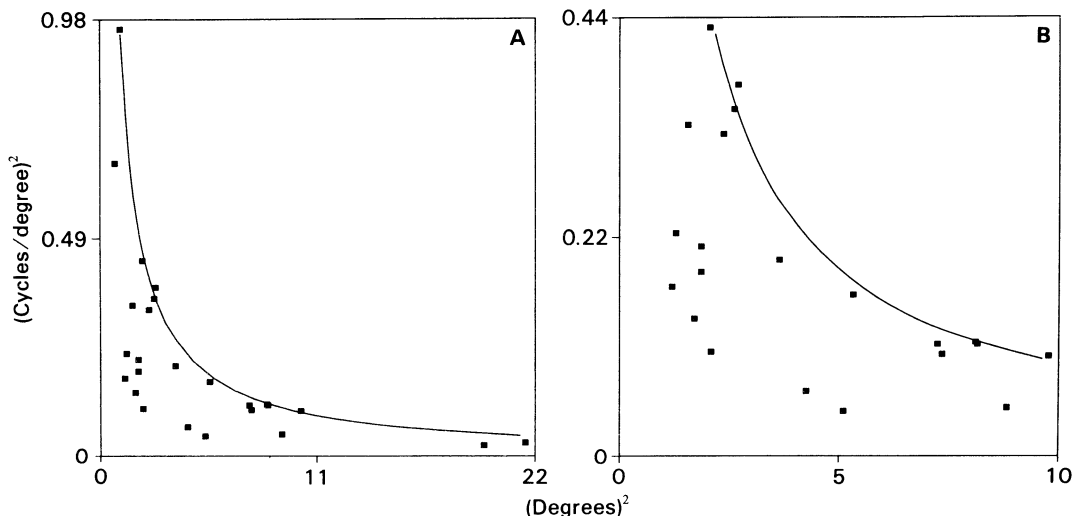


FIG. 11. The effective areas of the two-dimensional (2D) Gabor filter elliptic Gaussian terms as estimated from 2D spatial and spectral response profiles should be inverses. *A*: indeed, many of the points lie on or near the predicted solid hyperbola. *B*: a magnified view of the lower left portion of *A* reveals that many of the points lie inside the hyperbola. Because the hyperbola represents the best possible performance by any linear filter, this result indicates that some simple receptive fields have a spatial nonlinearity.<sup>2</sup>

The estimates of effective width and the effective length made using 2D spatial and spectral response profiles are illustrated in Fig. 10. The solid line in each part traces the predictions made by the 2D Gabor filter model. About one-half of the estimates of effective width lie close to the predicted hyperbolas (Fig. 10*A*); the remainder lie inside. Similar results were obtained for estimated effective length (Fig. 10*B*). If the reciprocal of the space domain effective widths and lengths are computed, the expectation converts to identity. The results of these calculations are illustrated in Fig. 10, *C* and *D*. Reasonably close agreement was obtained for both effective width ( $r = 0.80$ ) and effective length ( $r = 0.81$ ): many of the points lie on or near the predicted diagonal lines, but in both cases, some of the points lie below.

Estimates of effective area behave similarly (Fig. 11*A*). Three-fifths (15/25) of the points follow the predicted hyperbola reasonably well. Figure 11*B* provides a closer look at the region of Fig. 11*A* near the origin. In this illustration it can be seen that 10 of the points lie well inside (to the left) of the predicted hyperbola.

The results thus far demonstrate that all of the expected relationships except relative

spatial phase are reasonably well satisfied by 50–60% of the simple cells in our sample. These cells satisfy the constraint of linear 2D spatial summation, and the 2D Gabor filter is an excellent model of their 2D spatial and spectral response profiles.

The remaining cells show a characteristic deviation from the model; the observed effective lengths, widths, and areas are smaller in one domain than one would expect given the observations made in the reciprocal domain. We therefore compared the extent to which these observations deviate from the predictions in the length and width directions. We may define the joint occupied length and width as the product of the effective occupied lengths and widths, in which case the 2D Gabor filter model predicts

$$\text{joint occupied width: } \pi a_s a_f = 1$$

$$\text{joint occupied length: } \pi b_s b_f = 1$$

Figure 12 illustrates a comparison of the observed joint occupied lengths and widths. The 2D Gabor filter model predicts that both of these quantities should equal one and that all of the points should lie on the asterisk. The diagonal line in this case represents the prediction of a simple hypothesis; deviation

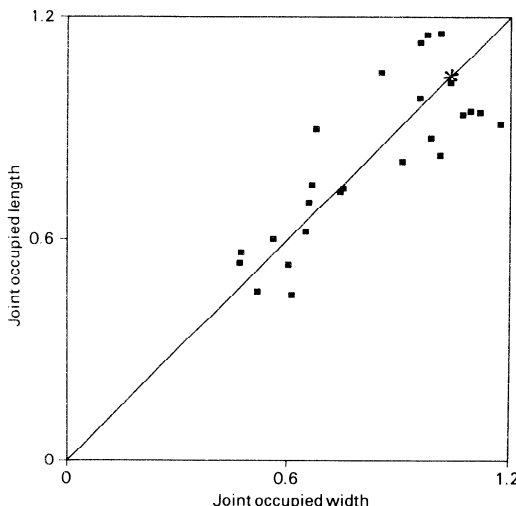


FIG. 12. Any mechanism invoked to explain the observed deviation from the predictions of the two-dimensional (2D) Gabor filter model must operate in 2 spatial dimensions. This figure compares the degree of deviation along the width and length axes of the receptive fields. The 2D Gabor filter model predicts that the joint occupied widths and lengths both equal unity (marked by an asterisk). Those receptive fields exhibiting deviations from this prediction do so to an equivalent degree in both dimensions (*diagonal line*). The correlation between the observed deviations is 0.81.

from the model is the same in both the length and width directions. The observations are distributed about the diagonal line, and there is reasonably good correlation ( $r = 0.81$ ). Thus any mechanism invoked to explain the deviations from the 2D Gabor filter model must operate in two spatial dimensions equivalently.

In summary, 2D spatial response profiles can be fully described as 2D Gabor filters. Statistical evaluation of the residual error reveals that the differences between 2D spatial response profiles and 2D Gabor filters are indistinguishable from random error. Similarly, 2D spectral response profiles can be fully described as 2D Gabor filters. No statistical evaluation of the residual error was performed, but very few 2D spectral response profiles exhibited visible deviations from 2D Gabor filter amplitude spectra. In general, the spatial and spectral parameters of the fitted 2D Gabor filters are in agreement, in support of the hypothesis of 2D linear spatial summation. In particular, modulation spatial frequency and orientation, elliptic Gaus-

sian size and shape, and relative orientation are largely in agreement. There are two notable exceptions. Estimates of relative spatial phase are largely uncorrelated. Estimates of elliptic Gaussian size do not agree in some cases.

## DISCUSSION

In virtually every case, a 2D Gabor filter could be found that accurately described the simple cell 2D spatial and spectral response profiles in our small population. In the space domain, the differences between the data and the fits were statistically indistinguishable from random error in most cases; in the frequency domain, there was no visible systematic structure in the residual error surfaces in most cases. All variations in the 2D spatial and spectral response profiles described in the preceding papers (19, 20) were easily captured by the general expressions for the 2D Gabor filter, including noncanonical spatial phase angles and Cartesian separable and nonseparable response profiles. In general, these results provide convincing empirical support for Marcelja's original hypothesis (26) and Daugman's extension of it to two spatial dimensions (7).

The 2D Gabor filter has many free parameters and is a remarkably flexible functional form. Degenerate decompositions include impulsive receptive fields (as the elliptic Gaussian vanishes) and pure sinusoids (as the elliptic Gaussian becomes infinite) among others. However, this filter cannot fit everything; the circularly symmetric difference of Gaussian's structure characteristic of retinal ganglion cell receptive fields (35) is an obvious example. There are many other conceivable forms a receptive field might assume that a 2D Gabor filter model cannot support: aperiodic zero crossings, curved or nonparallel subregions, and central subregions with lower amplitude than flanking subregions. We have observed neither receptive fields with these characteristics nor any receptive field having a form not reasonably well matched by 2D Gabor filters.

In the course of this work, we have encountered several unanticipated degrees of freedom in the spatial organization of simple receptive fields. Simple receptive fields are found in many relative spatial phase angles,

rather than in just sine and cosine phase. The 2D spatial response profiles frequently exhibit staggered subregions, and the 2D spectral response profiles frequently exhibit nonradial elongation. The general expression for the 2D Gabor filter accommodates these observations in a natural way, as translations and rotations of the spatial modulation term with respect to the Gaussian envelope.

Previously, we (32) and others (21, 22, 31) have observed simple receptive fields in cat striate cortex composed of many (up to six) spatially discrete, periodic subregions. Although we did not observe any "periodic" simple cells in the present study, we anticipate that the 2D Gabor filter will describe these receptive fields equally well.

The 2D Gabor filter's inherent flexibility may confer decided advantages on the system that employs it. Because its parameters are continuously variable, one imagines that the system can be fine-tuned according to the environment in which the organism finds itself, either through early visual experience (18) or by continual reconfiguration throughout the animal's lifetime (14). Simple receptive-field spatial structure can be completely specified with eight numbers, and this may lead to a representational economy in the system responsible for its specification. Further economy might be obtained by establishing a small set of repetitive rules that generate sets receptive field parameters in a neighborhood (a multidimensional loop).

There are an infinite number of 2D Gabor filters, but clearly only some of them can be expressed in cat striate cortex. Which ones are represented is a question that can be addressed with a large scale, systematic application of the methods described in these papers. A question of somewhat greater conceptual consequence is why is any particular subset of 2D Gabor filters is chosen.

Using Daugman's generalization (7) of Gabor's concepts (16), we may think of simple receptive fields as occupying hypervolumes in a four-dimensional information space, the coordinates of which specify spatial position in 2D and spatial frequency position in 2D. The receptive fields we observe are projections from this space onto the two familiar 2D spaces. Figure 13 illustrates  $1/e$  isoamplitude contour around the elliptic Gaussian terms of the fitted 2D Gabor filters

from subsets of our population in both the 2D space domain and the 2D spatial frequency domain. Figure 13, *A* and *B*, illustrates the placements of the space domain elliptic Gaussian in the visual field according to the eccentricities determined at the time of the experiments. Figure 13, *C* and *D*, illustrates placements in the 2D spatial frequency domain determined by 2D spectral response profiles.

At any given retinal eccentricity (Fig. 13, *A* and *B*), there is considerable variation in the sizes, orientations, and aspect ratios of the Gaussians. Similarly, at any given location in the spatial frequency domain (Fig. 13, *C* and *D*) there is similar variability. The known correlations of receptive-field size with retinal eccentricity and spectral eccentricity are reflected in these projections, even in this small population of cells. There does not appear to be a single sampling strategy (23) for information in the 4D space. To determine what the strategies actually are, a much larger sample of profiles are required.

#### *2D spatial response linearity*

The 2D Gabor filter hypothesis rests firmly on the assumption of 2D spatial response linearity, but our evaluation of this conjecture produced mixed results. Our approach to the issue of spatial response linearity differs somewhat from that of prior studies (2, 31), where 1D spatial response profiles and spatial frequency tuning curves were compared using the Fourier transform. This approach has both advantages and disadvantages. To its credit, it is simple to apply and makes no assumptions about the functional form of the response profiles in either domain. To its debit, it is difficult to make a quantitative assessment of the two curve's similarity, since a point-by-point comparison requires either that the data be taken at precisely reciprocal sampling intervals or that interpolation be used to obtain intermediate points not on the sampling net.

These problems are compounded when working in 2D. For a direct comparison of the two 2D response profiles via the Fourier transform, we would have had to sample on precisely reciprocal Cartesian grids at identical orientations. Indeed, this was our original intention and provided the motivation for the "near Cartesian" sampling grids used in

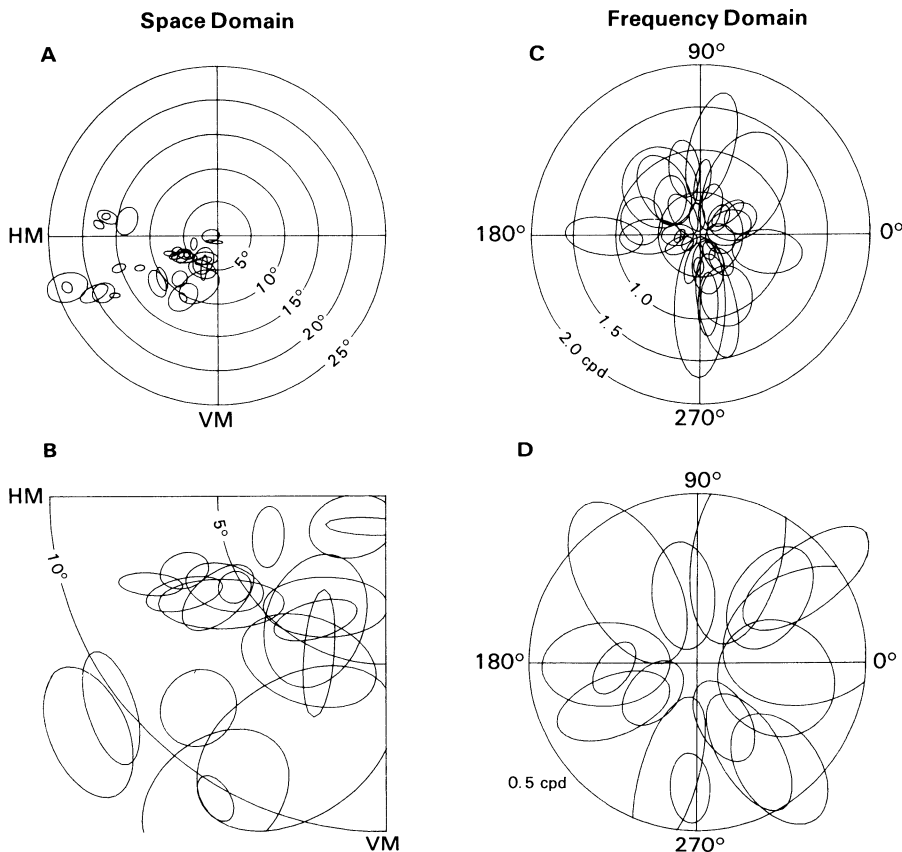


FIG. 13. Spatial and spectral response profiles can be thought of as projections from a four-dimensional information space onto the 2 familiar 2D spaces. *A* and *B*: 2D Gabor filter footprints ( $1/e$  isoamplitude contours around the elliptic Gaussian) in the 2D space domain. *C* and *D*: footprints in the 2D spatial frequency domain.

the second paper of this series (20). In practice, however, it proved impossible to generate perfectly Cartesian sampling grids at arbitrary orientations in the 2D spatial frequency domain. The resulting distortion of the sampling grids prevented direct comparison of 2D spatial and spectral response profiles using the 2D Fourier transform. Furthermore, even if we had solved or avoided these problems, it is not obvious that meaningful quantitative comparisons could have been made. Instead, we abandoned the direct Fourier transform approach in favor of the present method.

Our approach is based on the same principle as prior studies (the Fourier transform) and relies on independent measurements in the 2D space and spatial frequency domains. Receptive-field structure was determined by

finding the best fitting 2D Gabor filters and thus our method suffers from dependence on a specific functional form. The advantages are that once we have obtained the fit, we are left with fewer numbers to compare (the filter parameters), the comparison can be made across the entire population using a correlation analysis, and deviations from linearity can be parsed according to the effect each filter parameter has on receptive-field structure. Because the 2D Gabor filter model describes the data so well, the advantages of the present approach appear to outweigh the disadvantages.

The comparison of parameters obtained in this way show that most simple cells perform approximately linear 2D spatial summation. As an example, consider Fig. 14. The top row of Fig. 14 illustrates the 2D spatial response

profile and the 2D spectral response profile obtained from a single simple cell. A 2D Gabor filter describes each of these profiles well (see Figs. 2B and 3B). We have used the parameter estimates from the space domain fit to predict the spectral response profile, and the parameter estimates of the frequency domain fit to predict the spatial response profile, illustrated in the middle row. Not all of the parameters were used: we allowed the predicted spatial profile to reside in the same position as the original (shift invariance), and we allowed the two predicted profiles to retain the same relative phase as the original estimates.

The bottom row of Fig. 14 illustrates the residual error of the two predictions, which is everywhere small in both cases, but contains features typical of the errors we have observed. The predicted space domain profile is

both longer and wider than the original. The predicted frequency domain profile is slightly larger than the original in all directions, and the peak is shifted toward a slightly lower spatial frequency. However, comparison of the predicted and original response profiles is quite good.

In those cases where this reciprocal predictability was observed, 2D spatial response linearity obtains. Relative response amplitudes to small rectangular stimuli distributed over 2D of space can predict relative response amplitudes to drifting sinusoidal gratings of arbitrary spatial frequency and orientation. Relative response amplitudes to drifting sinusoidal gratings distributed over the 2D spatial frequency domain can predict relative response amplitudes to small rectangular stimuli of arbitrary spatial position (although a spatial phase angle must be as-

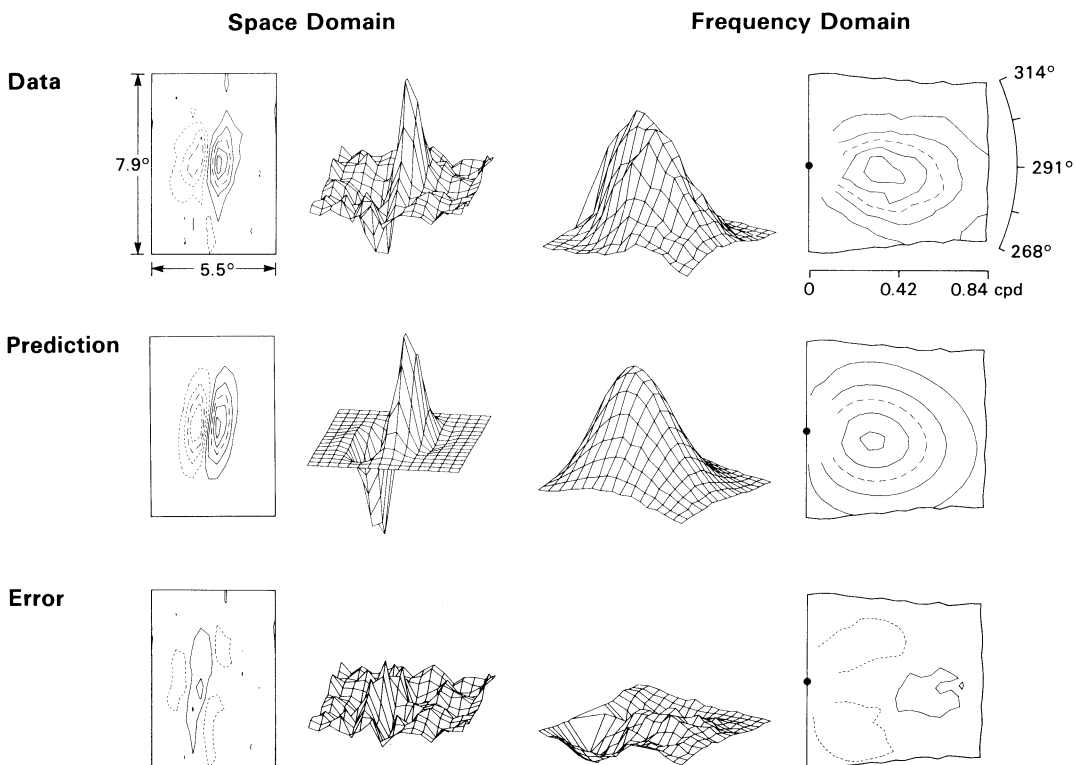


FIG. 14. In many cases, simple cell two-dimensional (2D) spatial and spectral response profiles are Fourier transform pairs, indistinguishable from 2D Gabor filters. Top row: the observed response profiles of a single cell. Middle row: the 2D spatial response profile predicted by the frequency domain data, and the 2D spectral response profile predicted by the space domain data, using the fitted 2D Gabor filters as intermediate steps in both cases. Bottom row: the error.

sumed). Presumably, either the 2D spatial or spectral response profile may be used to predict responses to stimuli of arbitrary complexity.

In those cases where the space domain and spatial frequency domain filter parameters do not agree, 2D spatial response linearity does not obtain. The largest observed deviations were in the sizes of the elliptic Gaussian (they were smaller than one would expect), and in the estimates of relative spatial phase. Furthermore, the mismatch in the sizes was of comparable magnitude in both spatial directions. However, even in these cases the estimates of elliptic Gaussian orientation and aspect ratio were in good agreement.

We may consider two general classes of explanations for the deviations from linearity observed in this study. First, the independent spatial and spectral measurements are, of necessity, not strictly comparable in several aspects. Notably, they differed in both their temporal structure and energies. Spectral stimuli were delivered at 4.0 Hz or less, whereas spatial stimuli were rarely delivered at <20 Hz. Further, the energy present in our spectral stimuli was orders of magnitude greater than that present in the small spots used for the spatial stimuli. One may presume that the operating point of each cell was quite different under these two forms of stimulation, and it is also likely that the spatial and temporal sensitivity functions are not completely orthogonal. It is easily conceived that either or both of these factors may have biased estimates of the sizes of the elliptic Gaussians away from the reciprocal relationship predicted by Gabor theory.

Another explanation may arise by considering each cell as a member of an interconnected cortical ensemble rather than an isolated entity with no connections other than those required to establish the 2D Gabor filter receptive-field structure. Other studies (10, 12, 13, 30) have reported spatial nonlinearities in some simple receptive fields, which may help to explain the deviations from linearity observed here.

Consider a simple cell having a 2D Gabor filter receptive field subjected in addition to weak inhibition from many other cortical cells (simple and/or complex) in the surrounding tissue, with the magnitude of the inhibition inversely proportional to distance

from the cell under consideration. The receptive fields of the neighboring cells will be close to the receptive field in space (by virtue of the retinotopic map, 17), orientation (by virtue of a columnar organization, 17), and spatial frequency (again, by virtue of a columnar organization, 38). Stimuli in 2D space or 2D spatial frequency delivered somewhat removed from the peak response loci of the cell under consideration would recruit inhibition from these cells. In the 2D space domain, cortical lateral inhibition would tend to diminish the observed size of 2D spatial response profiles. In the 2D spatial frequency domain, it would tend to diminish the observed size of 2D spectral response profiles. Consequently, when the two 2D profiles are compared assuming linearity, the observed size of the receptive fields will be less than expected given the results from the reciprocal domain.

The results presented in Fig. 12 of this paper suggest that any spatially nonlinear effect does not operate in a single specific direction, but rather in both directions at once. Thus we hypothesize no specific inhibitory connections between cells that depend on their respective physiological properties. It is possible that end-stopping (13), side-stopping (12), cross-orientation inhibition (30), and spatial frequency inhibition (10) are manifestations of a nonspecific set of lateral inhibitory connections which tends to restrict the occupied area of simple receptive fields in all directions in both domains simultaneously. We may, for instance, anticipate the discovery of "corner-stopping" in the space domain and a complementary phenomenon in the 2D spatial frequency domain. In terms of visual function this cortical lateral inhibition may serve to enhance the contrast of the image representation in the 4D information space.

#### *Encoding image features versus representing image structure*

2D Gabor filters not only provide a unifying mathematical expression of simple receptive-field structure, but also reveal a unifying concept underlying the design of this particular stage of early visual processing. Constrained by the fundamental uncertainty principle bounding simultaneous resolution in the 2D space and frequency domains, sim-

ple receptive fields are designed to achieve an optimal compromise with respect to resolution in these two reciprocal spaces.

But these filters possess certain properties that contradict current notions of how the brain analyzes the visual world. Most notable is the complete lack of spectral polar separability. This result contradicts the view that the brain attempts to explicitly encode the image parameters we ordinarily consider, such as orientation and spatial frequency.

There is an alternative view, based on the idea that visual receptive fields act as multidimensional filters. If the filter is linear, its output is related to its input by a convolution integral. These ideas are not new. What does not appear to be widely appreciated is what they imply. A neuron cannot encode any particular stimulus parameter, rather, it measures the similarity of the image to its receptive field.

If the visual system encodes stimulus parameters, then the output of a single neuron is ambiguous. It is possible to achieve a given firing rate within the neuron's dynamic range with an infinite number of stimuli, which vary in their respective spatiotemporal parameters (consider an isoresponse amplitude contour around a 2D spectral response profile). One consequence of the linear filter interpretation is that the output of a single neuron is unambiguous. It provides a measure of the similarity of the current local image structure to the structure of the neuron's receptive field.

Because the 2D Gabor filter serves so well as a model of the spatial organization of simple receptive fields, we may assume that the principle on which its derivation rests also applies to the behavior of simple cells as local spatial operators. Thus it is apparent that simple receptive fields are constructed to provide resolving power in both the space domain (as though they were responding to local image structure) and in the spatial frequency domain (as though they were responding to image structure over a larger scale). The 2D Gabor filter model resolves the "feature extraction" versus "spatial frequency filter" debate (1, 9, 11, 24) in favor of both positions.

Simple cells are selective for spatial position, but do not encode spatial position per se. Simple cells are selective for both orienta-

tion and spatial frequency, but do not encode either orientation or spatial frequency per se. Instead, the activity of each cell signals the amplitude of a coefficient, which simultaneously represents both spatial and spectral image structure in such a way that there is minimal joint uncertainty about this structure. Because 2D Gabor filters form a quasi-orthogonal complete basis set (3, 4), image information is preserved in a robust representation that makes explicit both spatial and spectral image attributes. Presumably, the set of simple cells spans the relevant stimulus dimensions, using a sampling logic, which remains to be uncovered, so that local image structure is represented at multiple scales and orientations, using a minimum number of cells.

Even though the 2D Gabor filter model describes much of the spatial behavior of simple cells, the description it provides is incomplete. Neither binocularity (17), nor any time-dependent behavior of simple cells are addressed. Direction asymmetry, selectivity, and velocity (or temporal frequency) selectivity are topics that require further theoretical treatment before we have a fully developed understanding of the filtering processes of the simple cell. The most straightforward approach might be simply to generalize the underlying uncertainty principle to three space, where the variables of interest are 2D space and time, with appropriate considerations for causality incorporated.

Vision is an information intensive sensory modality. We have shown that a particular information conservative optimization principle is utilized by the brain. These concepts may be of general utility in understanding the natural visual system and may find application in artificial vision as well.

#### ACKNOWLEDGMENTS

We are grateful to J. G. Daugman for many helpful discussions and useful suggestions and to Dr. Martin Pring for help with statistical issues.

This work was supported by National Institutes of Health Grant NEI-R01-EY-04638.

Present address of J. P. Jones: Division of Engineering Physics and Mathematics, Oak Ridge National Laboratory, Oak Ridge, TN 37830.

Received 19 May 1986; accepted in final form 7 July 1987.

## REFERENCES

- ALBRECHT, D. G., DEVALOIS, R. L., AND THORSELL, L. G. Visual cortical neurons: are bars or gratings the optimal stimuli? *Science Wash. DC* 207: 88-90, 1981.
- ANDREWS, B. W. AND POLLIN, D. A. Relationship between spatial frequency selectivity and receptive field profile of simple cells. *J. Physiol. Lond.* 287: 163-176, 1979.
- BASTIAANS, M. J. The expansion of an optical signal into a discrete set of Gaussian beams. *Optik* 57: 95-102, 1980.
- BASTIAANS, M. J. Gabor's expansion of a signal into Gaussian elementary signals. *Proc. IEEE* 68: 538-539, 1980.
- CACECI, M. S. AND CACHERIS, W. P. Fitting curves to data. *Byte* 9: 340-362, 1984.
- CAMPBELL, F. W., COOPER, G. F., AND ENROTH-CUGELL, C. The spatial selectivity of the visual cells of the cat. *J. Physiol. Lond.* 203: 223-235, 1969.
- DAUGMAN, J. G. Uncertainty relation for resolution in space, spatial frequency, and orientation optimized by two-dimensional visual cortical filters. *J. Opt. Soc. Am. 2*: 1160-1169, 1985.
- DEAN, A. F. The variability of discharge of simple cells in cat striate cortex. *Exp. Brain Res.* 44: 437-440, 1981.
- DEVALOIS, K. K., DEVALOIS, R. L., AND YUND, E. W. Responses of striate cortical cells to grating and checkerboard patterns. *J. Physiol. Lond.* 291: 483-505, 1979.
- DEVALOIS, K. K. AND TOOTELL, R. B. Spatial-frequency-specific inhibition in cat striate cortex cells. *J. Physiol. Lond.* 336: 359-376, 1983.
- DEVALOIS, R. L., ALBRECHT, D. G., AND THORSELL, L. G. Cortical cells: bar and edge detectors, or spatial frequency filters. In: *Frontiers of Visual Science*, edited by J. Cool and E. Smith. New York: Springer, 1978.
- DEVALOIS, R. L. AND THORELL, L. Periodicity of striate-cortex-cell receptive fields. *J. Opt. Soc. Am. 2*: 1115-1122, 1985.
- DREHER, B. Hypercomplex cells in the cat's striate cortex. *Invest. Ophthalmol. Visual Sci.* 11: 355-356, 1972.
- DELTMAN, G. M. AND FINKEL, L. H. Neuronal group selection in the cerebral cortex. In: *Dynamic Aspects of Neocortical Function*, edited by G. M. Edelman. New York: Wiley, 1984.
- FISHER, R. A. *Statistical Methods for Research Workers* (13th ed.). London: Oliver & Boyd, 1958.
- GABOR, D. Theory of communication. *J. IEE Lond.* 93: 429-457, 1946.
- HUBEL, D. H. AND WIESEL, T. N. Receptive fields, binocular interaction and functional architecture in the cat's visual cortex. *J. Physiol. Lond.* 160: 106-154, 1962.
- HUBEL, D. H. AND WIESEL, T. N. Receptive fields of cells in striate cortex of very young, visually inexperienced kittens. *J. Neurophysiol.* 26: 994-1002, 1963.
- JONES, J. P. AND PALMER, L. A. The two-dimensional spatial structure of simple receptive fields in cat striate cortex. *J. Neurophysiol.* 58: 1187-1211, 1987.
- JONES, J. P., STEPNOISKI, A., AND PALMER, L. A. The two-dimensional spectral structure of simple receptive fields in cat striate cortex. *J. Neurophysiol.* 58: 1212-1232, 1987.
- KULIKOWSKI, J. J. AND BISHOP, P. O. Silent periodic cells in the cat striate cortex. *Vision Res.* 22: 191-200, 1982.
- KULIKOWSKI, J. J. AND BISHOP, P. O. Linear analysis of the response of simple cells in the cat visual cortex. *Exp. Brain Res.* 44: 386-400, 1981.
- KULIKOWSKI, J. J., MARCELJA, S., AND BISHOP, P. O. Theory of spatial position and spatial frequency relations in the receptive fields of simple cells in the cat's striate cortex. *Biol. Cybern.* 43: 187-198, 1982.
- MACKAY, D. M. Strife over visual cortical function. *Nature Lond.* 289: 117-118, 1981.
- MAFFEI, L. AND FIORENTINI, A. The visual cortex as a spatial frequency analyzer. *Vision Res.* 13: 1255-1267, 1973.
- MARCELJA, S. Mathematical description of the responses of simple cortical cells. *J. Opt. Soc. Am.* 70: 1297-1300, 1980.
- MARR, D. *Vision*. San Francisco, CA: Freeman, 1982.
- MARR, D. AND HILDRETH, E. Theory of edge detection. *Proc. R. Soc. Lond. B Biol. Sci.* 207: 187-217, 1980.
- MOOD, A. M., GRAYBILL, F. A., AND BOES, D. C. *Introduction to the Theory of Statistics* (3rd ed.). New York: McGraw-Hill, 1974.
- MORRONE, M. C., BURR, D. C., AND MAFFEI, L. Functional implications of cross-orientation inhibition of cortical visual cells. I. Neurophysiological evidence. *Proc. R. Soc. Lond. B Biol. Sci.* 216: 335-354, 1982.
- MOVSHON, J. A., THOMPSON, I. D., AND TOLHURST, D. J. Spatial summation in the receptive fields of simple cells in the cat's striate cortex. *J. Physiol. Lond.* 283: 53-77, 1978.
- MULLIKIN, W. H., JONES, J. P., AND PALMER, L. A. Periodic simple cells in cat area 17. *J. Neurophysiol.* 52: 372-387, 1984.
- NELDER, J. A. AND MEAD, R. A simplex method for function minimization. *Comput. J.* 7: 308-313, 1965.
- PAPADIMITRIOU, C. H. AND STEIGLITZ, K. *Combinatorial Optimization*. Englewood Cliffs, NJ: Prentice-Hall, 1982.
- RODECK, R. W. AND STONE, J. Analysis of receptive fields of cat retinal ganglion cells. *J. Neurophysiol.* 28: 833-849, 1965.
- TOLHURST, D. J., MOVSHON, J. A., AND DEAN, A. F. The statistical reliability of signals in single neurons in cat and monkey visual cortex. *Vision Res.* 23: 775-785, 1983.
- TOLHURST, D. J., MOVSHON, J. A., AND THOMPSON, I. D. The dependence of response amplitude and variance of cat visual cortical neurons on stimulus contrast. *Exp. Brain Res.* 41: 414-419, 1981.
- TOOTELL, R. B. H., SILVERMAN, M. S., SWITKES, E., AND DEVALOIS, R. L. Spatial frequency columns in primary visual cortex. *Science Wash. DC* 218: 902-904, 1981.